





Cite this: *Phys. Chem. Chem. Phys.*,
2024, 26, 24041

Experimental investigation and thermodynamic modelling assessment of the $\text{AECl}_2\text{--NdCl}_3$ (AE = Sr, Ba) systems†

D. C. Alders,  D. J. Cette, R. J. M. Konings and A. L. Smith  *

The thermodynamic and thermo-physical properties of the binary salt systems $\text{AECl}_2\text{--NdCl}_3$ (AE = Sr, Ba) have been investigated using an experimental and modelling approach. The binary salt systems both include a single intermediate salt, *i.e.* $\text{Sr}_9\text{Nd}_5\text{Cl}_{33}$ and $\text{Ba}_3\text{Nd}_2\text{Cl}_{12}$, respectively. The structure of these intermediates has been investigated with X-ray diffraction (XRD). Furthermore, these systems exhibit mutual solubility of NdCl_3 in BaCl_2 and SrCl_2 . The investigation of these solid solutions has been performed using quenching experiments and subsequent post-characterisation by XRD. Phase diagram equilibria have also been investigated using differential scanning calorimetry (DSC). Using the aforementioned information on phase transitions, intermediate compound formation, and solid solubility, thermodynamic assessment of the systems has been performed using the CALPHAD method. The model for the Gibbs energy of the liquid solution is the quasi-chemical formalism in the quadruplet approximation, while the model for the Gibbs energy of the solid solutions is the two-sublattice polynomial model.

Received 30th April 2024,
Accepted 4th August 2024

DOI: 10.1039/d4cp01784f

rsc.li/pccp

1. Introduction

The molten salt reactor (MSR) is a nuclear reactor design that was selected by the Generation IV International Forum¹ as a promising concept for the next generation of reactors. For the safety assessment of such a reactor, a comprehensive understanding and modelling of the physical and chemical properties of the nuclear fuel is necessary. Many studies have already been conducted on the topic of fluoride-based reactors because of their appealing characteristics in terms of low vapour pressure and high thermochemical stability,^{2,3} but more recently chloride-based fuels have garnered attention as well.⁴ Compared to fluoride salts, chloride salts generally have a lower melting point, allowing for lower operating temperatures, and they show a higher solubility for actinides. During reactor operation, heat is generated by the fission reaction of a fissile isotope (^{235}U , ^{233}U , or ^{239}Pu), which produces fission products. The dissolution of these fission products in the molten chloride fuel makes it a multi-component system, thereby affecting its thermochemical and thermophysical properties. In order to predict the properties of such a multi-element system, extrapolation from the constituting binary or ternary sub-systems

can be used, but for this, the thermochemistry of the constituting binaries must first be comprehensively understood.

For fluoride salts, a large knowledge base of thermodynamic and thermophysical properties has been developed already in the framework of MSR development.⁵ For molten chlorides, however, the effect of fission products on properties such as melting behaviour, heat capacity, density or viscosity is less known and needs to be investigated. In particular, the effect on the thermodynamic properties of the melt of high-yield salt-soluble fission products such as barium, strontium and neodymium must be investigated. Neodymium is of additional interest, because it can also be used as a simulant for the hazardous plutonium due to its similar thermochemical behaviour in a salt mixture, as confirmed in this article. This work more specifically contributes to a better understanding of the effect of fission products in molten chlorides by modelling the thermochemical properties of the binary systems $\text{AECl}_2\text{--NdCl}_3$ (AE = Sr, Ba) using the CALPHAD (calculation of phase diagrams) method, based on literature and newly obtained experimental data.

Experimental investigations using X-ray diffraction, quenching experiments, and differential scanning calorimetry (DSC) were first performed to solve discrepancies noticed in the literature. Using those data as input, a CALPHAD model was then developed based on the quasi-chemical formalism in the quadruplet approximation for the liquid solutions, and a two-sublattice polynomial model for the solid solutions. In this process, mixing enthalpies of the liquid solution were also

Delft University of Technology, Faculty of Applied Sciences, Radiation Science & Technology Department, Mekelweg 15, 2629 JB Delft, The Netherlands.
E-mail: a.l.smith@tudelft.nl

† Electronic supplementary information (ESI) available: Experimental investigations and modelling of the thermochemistry of the $\text{AECl}_2\text{--NdCl}_3$ (AE = Sr, Ba) molten salt systems. See DOI: <https://doi.org/10.1039/d4cp01784f>



estimated, as these data have not been measured experimentally to this date, but constitute a key piece of information to develop physically accurate liquid models. To conclude this work, application calculations were performed to investigate the effect of the fission products Ba and Sr on the NaCl–NdCl₃ system, which serves as an analog to the fuel system NaCl–PuCl₃.

2. Experimental techniques

2.1. Sample preparation synthesis

For the experiments carried out in this work, BaCl₂ (Alfa Aesar, ultra-dry, 99.999% trace metals basis), SrCl₂ (Alfa Aesar, ultra-dry, 99.995% trace metals basis) and NdCl₃ (Alfa Aesar, ultra-dry, 99.9% trace metals basis) were used as delivered by the supplier. Due to the sensitivity of the salts towards oxygen and water, all sample preparation was carried out inside a glove box under dry argon atmosphere (H₂O, O₂ < 5 ppm).

Weighing was carried out using a Mettler-Toledo XPE105DR balance with a 0.01 mg uncertainty. Synthesis of intermediate compounds was conducted by mixing end-members compounds in the appropriate stoichiometric ratios in an agate mortar, followed by thermal treatment in a tubular furnace under argon flow for eight to twelve hours at a temperature of 850 K (Sr₉Nd₅Cl₃₃) or 950 K (Ba₃Nd₂Cl₁₂). The samples were heated inside a tightly closed stainless steel container, with an inner nickel liner to prevent the corrosive chlorides from interacting with the stainless steel.

Phase purity was analysed using X-ray diffraction (XRD) and melting point determination by differential scanning calorimetry (DSC). Using XRD, no additional phases were detected for any of the pure end-members. Using DSC, the melting points of the end-members were determined to be (1237 ± 5) K (BaCl₂), (1147 ± 5) K (SrCl₂) and (1031 ± 5) K (NdCl₃). These values are in good agreement with the values in the literature, which are reported as (1235 ± 1) K,⁶ (1147 ± 1) K,⁶ and (1032 ± 2) K,⁷ respectively.

The intermediate products were also analysed using XRD and in case there were still unreacted end-member reactants visible, the product was subjected to further heat treatment until the intermediate phase was obtained with high purity (> 99%).

2.2. X-ray diffraction (XRD)

XRD measurements were carried out using a panalytical X'pert pro diffractometer with a Cu-anode (0.4 mm × 12 mm line focus, 45 kV, 40 mA). Scattered X-ray intensities were measured with a real-time multi-step detector (X'Celerator). The angle 2θ was set to cover a range from 10° to 120°. Measurements were typically performed for 7–8 hours, with a step size of 0.0036° s⁻¹. Refinement of the measured XRD data was performed by applying the method Le Bail,⁸ using the FullProf software, Version 5.10.⁹

2.3. Differential scanning calorimetry (DSC)

The invariant temperatures in the investigated systems were measured using a Setaram multi-detector high-temperature calorimeter (MHTC-96 type) equipped with a 3D heat flux

DSC module, capable of measuring up to 1673 K. Sample preparation was done by mixing end-members BaCl₂ or SrCl₂ with NdCl₃ in the desired stoichiometric ratio. The samples were contained in a nickel liner, which in turn was contained in a tightly closed stainless steel crucible.¹⁰ Equilibration of the sample was done in the calorimeter itself during the first heating cycle by heating the mixtures to a temperature above the melting points of both end members. Invariant equilibria were collected on the subsequent cycles.

The temperature was monitored throughout the experiments by a series of interconnected S-type thermocouples. The temperature on the heating ramp (10 K min⁻¹) was calibrated and corrected for the effect of the heating rate by measuring the melting points of standard high purity metals (In, Sn, Pb, Al, Ag, Au) at 2–4–6–8–10–12 K min⁻¹. The calibration procedure was performed as recommended by Höne *et al.*¹¹ and Gatta *et al.*¹² The transition temperatures in the AECl₂–NdCl₃ phase diagrams (AE = Sr, Ba) were derived on the heating ramp as the onset temperature using tangential analysis of the recorded heat flow. The liquidus temperature of mixtures was derived from the peak extremum of the last thermal event. The uncertainty on the measured temperatures is estimated to be ±5 K for pure compounds and ±10 K for mixtures.

2.4. Investigation of solid solutions

The existence and stability range of solid solutions in the investigated systems were investigated in this work using quenching experiments. The quenching samples consisted of stoichiometric mixtures of the end-members, thoroughly mixed using a pestle and mortar before insertion inside a nickel liner in a tightly closed stainless steel crucible. During the experiments, the samples were heated to a temperature of 973 K and equilibrated at this temperature for at least two hours, after which they were dropped into a water bath to freeze the phases stable at high temperature.

The furnace used for quenching is an MTI split vertical quenching tube furnace (OTF-1500X-80-VTQ), which contains an electromagnet that holds the sample in the heated part of the furnace. When the sample is at the desired temperature and has reached equilibrium, the electromagnet is shut off and the sample drops into a water bath. Due to the double containment of the sample of nickel inside stainless steel, the sample stays water-free during this experiment.

3. Thermodynamic modelling

The thermodynamic modelling assessment of the molten salt systems was performed with the CALPHAD method¹³ using the FactSage software, Version 8.2.¹⁴ Both literature and experimental data obtained in this work were used to adjust the excess parameters of the Gibbs energy functions of the phases present in the systems.

3.1. Stoichiometric compounds

The Gibbs energy function ($G(T)$, kJ mol⁻¹) for stoichiometric compounds is dependent on the standard enthalpy of



formation ($\Delta_f H_m^\circ(298)$, kJ mol^{-1}), the standard entropy ($S_m^\circ(298)$, $\text{J mol}^{-1} \text{K}^{-1}$) at the reference temperature of 298.15 K and the heat capacity ($C_{p,m}(T)$, $\text{J mol}^{-1} \text{K}^{-1}$) as shown in eqn (1).

$$G(T) = \Delta_f H_m^\circ(298) - S_m^\circ(298)T + \int_{298}^T C_{p,m}(T) dT - T \int_{298}^T \frac{C_{p,m}(T)}{T} dT \quad (1)$$

The isobaric heat capacity $C_{p,m}$ is expressed as a polynomial that takes the form of eqn (2).

$$C_{p,m}(T) = a + bT + cT^2 + dT^{-2} \quad (2)$$

The compounds in the investigated systems are two end-members and two intermediates. The thermodynamic data for these are listed in Table 1. The thermodynamic functions for NdCl_3 were taken from the critical review by Konings and Kovács.⁷ The thermodynamic functions for BaCl_2 were taken from the IVTAN thermochemical database,¹⁵ to be consistent with our earlier work.¹⁶ The thermodynamic functions for SrCl_2 were taken from the JANAF thermochemical tables.⁶ A polymorphic transition is reported in the aforementioned tables for SrCl_2 with a transition enthalpy of 6 kJ mol^{-1} that was not included in the current thermodynamic modelling assessment. This transition is a second-order transition, from a cubic structure to a slightly distorted cubic structure, that does not appear in phase equilibria measurements, as further elaborated on in 6. The thermodynamic functions of NaCl , used in the assessment of the ternary systems, were taken from van Oudenaeren *et al.*,¹⁷ who reviewed the available thermodynamic data in their work. The heat capacity of the intermediate compounds in this work was obtained through the Neumann–Kopp rule.

3.2. Liquid solution

The excess Gibbs energy terms of the liquid solution are modelled using the quasi-chemical formalism in the quadruplet approximation as proposed by Pelton *et al.*¹⁹ which has proven

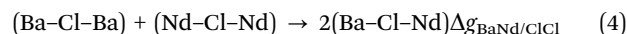
Table 2 Coordination numbers used in the CALPHAD model presented in this work

A	B	$Z_{AB/ClCl}^A$	$Z_{AB/ClCl}^B$	$Z_{AB/ClCl}^{Cl}$
Ba	Ba	6	6	3
Sr	Sr	6	6	3
Nd	Nd	6	6	2
Ba	Nd	6	3	1.5
Ba	Sr	6	6	3
Sr	Nd	6	6	1.9

to be well-adapted to molten chloride and fluoride systems. This description assumes the existence of quadruplets in the liquid, allowing for the modelling of short-range ordering. This formalism allows for the selection of the composition of maximum short-range ordering through its cation–cation coordination numbers, corresponding to the minimum of the Gibbs energy that is often found near the composition of the lowest eutectic. By fixing these numbers, the anion–anion coordination number is also obtained through eqn (3), where q_i are the charges of the respective ions. The cation–cation coordination numbers used in this work are presented in Table 2.

$$\frac{q_A}{Z_{AB/ClCl}^A} + \frac{q_B}{Z_{AB/ClCl}^B} = 2 \cdot \frac{q_{Cl}}{Z_{AB/ClCl}^{Cl}} \quad (3)$$

The excess parameters that are optimized are those related to the second-nearest neighbour exchange reaction as given in eqn (4), where the associated change in Gibbs energy ($\Delta g_{BaNd/ClCl}$, J mol^{-1}) is expressed as eqn (5).



$$\Delta g_{BaNd/ClCl} = \Delta g_{BaNd/ClCl}^0 + \sum_{i \geq 1} g_{BaNd/ClCl}^{i0} \lambda_{BaNd/ClCl}^i + \sum_{j \geq 1} g_{BaNd/ClCl}^{0j} \lambda_{NdBa/ClCl}^j \quad (5)$$

In eqn (5) the terms $\Delta g_{BaNd/ClCl}^0$, $g_{BaNd/ClCl}^{i0}$ and $g_{BaNd/ClCl}^{0j}$ are composition-independent coefficients that may depend on temperature. The composition dependence of the Gibbs energy

Table 1 Thermodynamic functions used in the CALPHAD model in this work. Optimized values are marked in bold

Compound	$\Delta_f H_m^\circ(298)$ (J mol^{-1})	$S_m^\circ(298)$ ($\text{J K}^{-1} \text{mol}^{-1}$)	$C_{p,m}(T)$ ($\text{J K}^{-1} \text{mol}^{-1}$) = $a + bT + cT^{-2} + dT^2$				Temperature range (K)	Source
			<i>a</i>	<i>b</i>	<i>c</i>	<i>d</i>		
α - $\text{BaCl}_2(\text{s})$	−855 200	123.7	69.371	0.01912548		5882.698	2.499235 $\times 10^{-9}$	[298–1198] 15
β - $\text{BaCl}_2(\text{s})$	−837 800	138.22	131					[1198–1234]
$\text{BaCl}_2(\text{l})$	−821 950	151.07	109					[1234–2500]
$\text{SrCl}_2(\text{s})$	−828 850.4	114.809	79.48261	−0.001792036	−440 859.7	1.798911 $\times 10^{-5}$		[298–600] 6
			194.5439	−0.246728	−8 159 846	0.0001661617		[600–1000]
			123.0096					[1000–1147] This work
$\text{SrCl}_2(\text{l})$	−812 629	128.95145858762	104.6					[1147–2000] 6
$\text{NdCl}_3(\text{s})$	−1 040 900	153.5	109.084	0.016406	−1 309 950			[298–1032] 7
$\text{NdCl}_3(\text{l})$	150							[1032–3000]
$\text{NaCl}(\text{s})$	−411 260	72.15	47.72158	0.0057	−882.996	1.21466 $\times 10^{-5}$		[298–1074] 17
$\text{NaCl}(\text{l})$	−390 853	83.30249	68					[1074–2500] 18
$\text{Sr}_9\text{Nd}_5\text{Cl}_{33}(\text{s})$	−12 782 000	1800	737.36	0.91178	−14 478 000			[298–1500] This work
$\text{Ba}_3\text{Nd}_2\text{Cl}_{12}(\text{s})$	−4 641 500	682	486.281	0.09018844	−2602251.9	7.2 $\times 10^{-9}$		[298–1500]
$\text{Na}_3\text{Nd}_5\text{Cl}_{18}(\text{s})$	−6 478 000	983.845	714.332	0.042932	−7 577 460	6.56 $\times 10^{-5}$		[298–1500]



is apparent through $\chi_{\text{BaNd/ClCl}}$ as these are defined as per eqn (6). In this equation X_{AA} is the cation–cation pair fraction, or the molar fraction of the quadruplet containing two cations A. For this binary system, $\{X_{\text{AA}} + X_{\text{AB}} + X_{\text{BB}}\}$ is equal to one.

$$\chi_{\text{AB/ClCl}} = \frac{X_{\text{AA}}}{X_{\text{AA}} + X_{\text{AB}} + X_{\text{BB}}} \quad (6)$$

The Gibbs energy functions used in this work to describe the liquid solutions are given in eqn (7) and (8) for the SrCl_2 – NdCl_3 and BaCl_2 – NdCl_3 systems, respectively.

$$\Delta g_{\text{SrNd/ClCl}} = -1800 - 2.5T + (1.5T)\chi_{\text{SrNd/ClCl}} + (-3300 + 4T)\chi_{\text{NdSr/ClCl}} \quad (7)$$

$$\Delta g_{\text{BaNd/ClCl}} = -6500 - 0.7T + (-7000 + 8T)\chi_{\text{NdBa/ClCl}} \quad (8)$$

3.3. Solid solution modelling

The thermodynamic description of solid-solutions is done using the two-sublattice polynomial model to be consistent with the description of the JRC Molten Salt Database (JRCMSD).²⁰ The Gibbs Energy function $G(T)$ (J mol^{-1}) of the solid-solution is given in eqn (9).

$$G(T) = X_{\text{A}} \cdot G_{\text{A}}^0 + X_{\text{B}} \cdot G_{\text{B}}^0 + X_{\text{A}}RT \ln X_{\text{A}} + X_{\text{B}}RT \ln X_{\text{B}} + \Delta G_{\text{m}}^{\text{excess}} \quad (9)$$

In the above equation, G_i^0 are the end-member molar Gibbs energies, and X_i are the site molar fractions of the end-members SrCl_2 or BaCl_2 (A) and NdCl_3 (B), respectively. The third and fourth terms in eqn (9) represent the configurational entropy. The excess Gibbs energy, present in eqn (9) as $\Delta G_{\text{m}}^{\text{excess}}$ (in J mol^{-1}), is defined as per eqn (10).

$$\Delta G_{\text{m}}^{\text{excess}} = \sum_{i,j \geq 1} y_{\text{A}}^i y_{\text{B}}^j L_{\text{AB}}^{ij} \quad (10)$$

The term L_{AB}^{ij} in eqn (10) is an interaction coefficient that can be a function of temperature if necessary. The equivalent site fractions y_{A} and y_{B} are charge equivalent site fractions. In this work, these fractions are y_{Ba} (resp. y_{Sr}) and y_{Nd} , as defined by eqn (11) and (12):

$$y_{\text{Ba}} = \frac{2X_{\text{Ba}}}{2X_{\text{Ba}} + 3X_{\text{Nd}}} \quad (11)$$

$$y_{\text{Nd}} = \frac{3X_{\text{Nd}}}{3X_{\text{Nd}} + 2X_{\text{Ba}}} \quad (12)$$

The Gibbs energy function used in this work to describe the solid solutions in the BaCl_2 – NdCl_3 system is given in eqn (13), where NdCl_3 is soluble in the high-temperature cubic phase β - BaCl_2 . For the modelling of the SrCl_2 – NdCl_3 system, separate solid solution descriptions were used to model the solubility of NdCl_3 in the cubic SrCl_2 (eqn (15)) and the solubility of SrCl_2 in the hexagonal NdCl_3 (eqn (14)).

$$\Delta G_{\text{m,cubic(Ba,Nd)}}^{\text{excess}} = y_{\text{Ba}}^2 y_{\text{Nd}} (-12\,110 + 5T) + y_{\text{Ba}} y_{\text{Nd}}^2 (7000) \quad (13)$$

$$\Delta G_{\text{m,cubic(Sr,Nd)}}^{\text{excess}} = y_{\text{Sr}} y_{\text{Nd}} (9000) + y_{\text{Sr}}^2 y_{\text{Nd}} (20\,000) \quad (14)$$

$$\Delta G_{\text{m,hexagonal(Nd,Sr)}}^{\text{excess}} = y_{\text{Sr}} y_{\text{Nd}} (-4000) + y_{\text{Sr}} y_{\text{Nd}}^2 (20\,000) \quad (15)$$

4. Results and discussion

The phase diagrams of the salt systems AECl_2 – NdCl_3 ($\text{AE} = \text{Sr}, \text{Ba}$) have been investigated experimentally in this work through the use of XRD, quenching experiments and DSC. The mixing enthalpy of the systems has been estimated using the estimation method of Davis and Rice,²¹ as explained in a previous work.¹⁶ We refer the reader to the latter paper for a detailed explanation of the estimation method applied to derive the mixing enthalpies. Additionally, an assessment of Nd as a simulant for Pu is presented in Section 4.1, through the comparison with other commonly used simulant elements in Ce and U.

In the SrCl_2 – NdCl_3 system, the intermediates $\text{Sr}_4\text{NdCl}_{11}$ (space group $P2_1/m$) and $\text{Sr}_9\text{Nd}_5\text{Cl}_{33}$ (space group $R\bar{3}$), as well as a solid solution $\text{Sr}_{1-x}\text{Nd}_x\text{Cl}_{2+x}$, have been identified by Hodorowicz *et al.*²² Experimental measurement of invariant equilibria has been reported by Morozov *et al.*²³ and Vogel *et al.*²⁴ No intermediates have been reported in the literature on the BaCl_2 – NdCl_3 system. However, Meyer *et al.*²⁵ have reported a compound with the chemical formula $\text{Ba}_9\text{Nd}_6\text{Cl}_{34}\text{O}$. This compound could correspond to the intermediate $\text{Ba}_3\text{Nd}_2\text{Cl}_{12}$ instead, as is the case in the analogous BaCl_2 – CeCl_3 system.¹⁶ Measurements of invariant equilibria have been reported by Morozov *et al.*²³ and Vogel *et al.*²⁴

4.1. Simulant systems NaCl – MCl_3 ($\text{M} = \text{Ce}, \text{Nd}, \text{U}$)

To assess the potential of neodymium as a simulant for plutonium in the context of molten chlorides, a comparison between systems consisting of NaCl with NdCl_3 , CeCl_3 and UCl_3 is presented in this section. Thermodynamic models for these systems have been used to calculate phase diagrams, which were then compared to the experimental phase diagram data on the NaCl – PuCl_3 system presented by Bjorklund *et al.*²⁶ as shown in Fig. 1.

The thermodynamic model of the NaCl – NdCl_3 system was optimized based on data from the literature in this work, as detailed in 8. For the thermodynamic model of the NaCl – CeCl_3 system, we refer the reader to a previous work.¹⁶ The thermodynamic model of the system NaCl – UCl_3 was taken from Beneš and Konings,²⁷ with the addition of the intermediate NaU_2Cl_7 as suggested by Yingling *et al.*²⁸ Fig. 1 shows that both the eutectic compositions and eutectic temperatures of the CeCl_3 –system and UCl_3 –system deviate significantly from the experimental data in the PuCl_3 –system. Moreover, the temperature of the liquidus on the right side of the eutectic, is consistently higher than that of the NaCl – PuCl_3 system, mainly due to the difference in melting points between the compounds.

Fig. 1 also shows that the model of the NaCl – NdCl_3 system reproduces the experimental data for the NaCl – PuCl_3 system



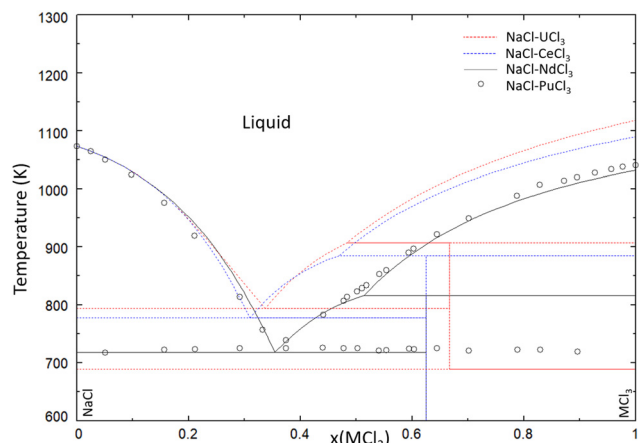


Fig. 1 Calculated phase diagrams of the systems NaCl–NdCl₃ (solid black line), NaCl–CeCl₃ (dashed blue line) and NaCl–UCl₃ (dashed red line), compared to the experimental data on the NaCl–PuCl₃ system (open black circles) presented by Bjorklund *et al.*⁷

very well. The main difference between these two systems, is that the intermediate Na₃Nd₅Cl₁₈ ($x(\text{NdCl}_3) = 0.625$) does not have a known Pu-analog. This does not significantly influence the temperature of the liquidus, however, and therefore makes Nd an excellent simulant to describe the melting behaviour of Pu-systems. The SrCl₂–NdCl₃ and BaCl₂–NdCl₃ systems are subsequently investigated in this work, which can give insights into the melting behaviours of the SrCl₂–PuCl₃ and BaCl₂–PuCl₃ systems, respectively.

4.2. Intermediates Sr₉Nd₅Cl₃₃ and Ba₃Nd₂Cl₁₂

Both systems SrCl₂–NdCl₃ and BaCl₂–NdCl₃ contain one intermediate compound with composition Sr₉Nd₅Cl₃₃ and Ba₃Nd₂Cl₁₂, respectively. The intermediate phase Sr₄NdCl₁₁ as suggested by Hodorowicz *et al.*²² was not observed in any of our synthesis attempts. The intermediate Sr₉Nd₅Cl₃₃ (hexagonal in space group *R*3̄) was successfully synthesised, and the profile

refinement is shown in Fig. 2. The obtained refined cell parameters are compared to those presented by Hodorowicz *et al.* in Table 3, and these are in good agreement with each other (Fig. 3).

The intermediate Ba₃Nd₂Cl₁₂ has not been reported in the literature before, but Meyer *et al.*²⁵ do suggest the existence of a compound with the same stoichiometric ratio of barium to neodymium, *i.e.* Ba₉Nd₆Cl₃₄O. In our previous work on the analogous BaCl₂–CeCl₃ system,¹⁶ we encountered a similar situation where the crystallographic information published by Meyer *et al.* for Ba₉Ce₆Cl₃₄O agreed very well with our synthesised compound Ba₃Ce₂Cl₁₂. We therefore conclude that the same occurs here, and the intermediate Meyer *et al.* identified as Ba₉Nd₆Cl₃₄O is actually the intermediate Ba₃Nd₂Cl₁₂ (tetragonal in space group *I*4/*m*) as presented in this work. The refined lattice parameters obtained in this work are shown in Table 4, and are compared to the one presented by Meyer *et al.*,²⁵ as well as the values reported for Ba₃Ce₂Cl₁₂ in the literature. The lattice parameters of Ba₃Nd₂Cl₁₂ are smaller than those of Ba₃Ce₂Cl₁₂, as expected since the crystal radius of Nd³⁺ is smaller than that of Ce³⁺.²⁹ There is a slight discrepancy between the values reported by Meyer *et al.* and those obtained in this work, particularly regarding the lattice parameter *c*. However, as shown in Table 4, this is also the case for the intermediate Ba₃Ce₂Cl₁₂, leading us to believe that the intermediate observed in this work is indeed an analog to Ba₃Ce₂Cl₁₂. Meyer *et al.* suggested the presence of an oxygen ion in this structure to satisfy charge conditions, but we believe that two chlorine ions are more likely. The reader is referred to the previously mentioned work by Alders *et al.*¹⁶ for further details on the crystallography of this compound.

4.3. Solid-solutions – Sr_{1–x}Nd_xCl_{2+x}

In their investigation of the SrCl₂–NdCl₃ system, Hodorowicz *et al.*²² found that NdCl₃ is soluble in the cubic crystal structure of SrCl₂ (space group *Fm*3̄*m*) with a maximum of approximately

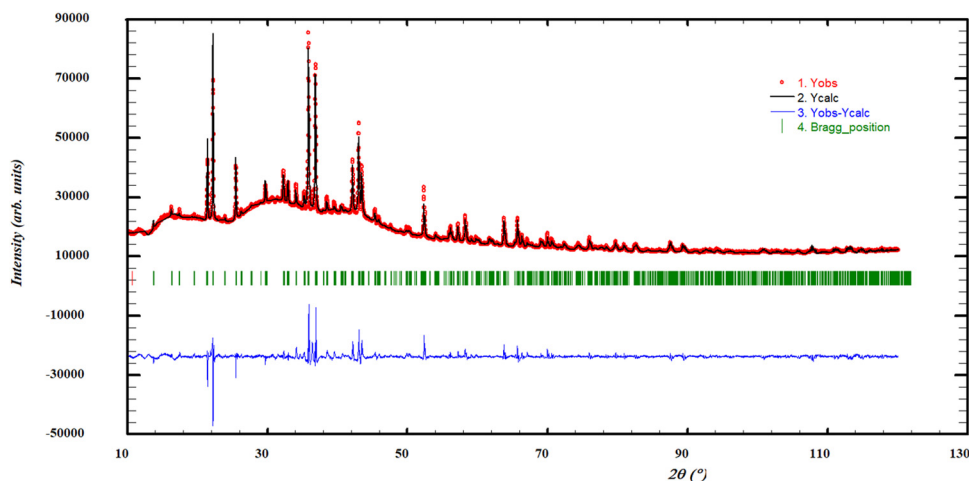


Fig. 2 Profile refinement of the intermediate salt Sr₉Nd₅Cl₃₃ using the structural model by Hodorowicz *et al.*²² The observed intensity (Y_{obs} , red) is plotted along with the calculated intensity from the refinement (Y_{calc} , black), and the difference between the two is shown ($Y_{\text{obs}} - Y_{\text{calc}}$, blue). The angles at which reflections occur are shown as well (Bragg positions, vertical lines). Measurement at $\lambda = \text{Cu-K}\alpha$.



Table 3 Comparison between cell parameters obtained for intermediate $\text{Sr}_9\text{Nd}_5\text{Cl}_{33}$ (space group $R\bar{3}$) in this work and in the literature

Source	a, b (Å)	c (Å)	V (Å ³)
This work	12.899(1)	24.858(2)	4136(2)
Hodorowicz <i>et al.</i> ²²	12.908(6)	24.82(1)	4135(5)

18% NdCl_3 . The existence of this solid solution is confirmed in this work with quenching and post-XRD measurements. Stoichiometric mixtures of SrCl_2 and NdCl_3 of compositions $x(\text{NdCl}_3) = 0, 0.05, 0.1$ and 0.15 were quenched from 923 K. All mixtures showed a single phase solid solution. The profile refinements of the collected XRD data are reported in the supplementary information to this work, and the evolution of the lattice parameters in Fig. 5.

In Fig. 4, a refinement of the post-XRD at $x(\text{NdCl}_3) = 0.1$, quenched from 850 K, is shown, indicating a single-phase solid solution at this composition. In contrast to the findings of Hodorowicz *et al.*, the cell volumes calculated with the refined lattice parameters from the profile refinements do not obey a decreasing linear trend, but instead seem to fluctuate around an average value, as seen in Fig. 5. Based on the DSC data obtained in this work, shown in Section 4.7.1, we are inclined to conclude that the solid solution is stable up to approximately 20% NdCl_3 , as the peritectic transition observed at approximately 890 K disappears at lower concentrations. This is in line with the 18% solubility limit as reported by Hodorowicz *et al.*²²

4.4. Solid-solutions – $\text{Ba}_{1-x}\text{Nd}_x\text{Cl}_{2+x}$

Solid solutions of CeCl_3 in the high-temperature cubic phase of BaCl_2 (space group $Fm\bar{3}m$) have been observed previously by Alders *et al.*¹⁶ in the BaCl_2 – CeCl_3 system. Due to the similarities between CeCl_3 and NdCl_3 ($r_{\text{Ce}(3+),\text{VI}} = 1.01$ Å, $r_{\text{Nd}(3+),\text{VI}} = 0.98$ Å²⁹), we expect a similar solid solution to also form in this system. Additionally, the invariant points measured by DSC between

Table 4 Comparison between cell parameters obtained for intermediates $\text{Ba}_3\text{RE}_2\text{Cl}_{12}$ (RE = Ce, Nd) (space group $I4/m$) in this work and the literature

Source	Compound	a, b (Å)	c (Å)	V (Å ³)
This work	$\text{Ba}_3\text{Nd}_2\text{Cl}_{12}$	11.304(7)	21.635(3)	2765(2)
Meyer <i>et al.</i> ²⁵	$\text{Ba}_9\text{Nd}_6\text{Cl}_{34}\text{O}$	11.329(5)	21.676(7)	2782(4)
Alders <i>et al.</i> ¹⁶	$\text{Ba}_3\text{Ce}_2\text{Cl}_{12}$	11.363(1)	21.547(6)	2782(2)
Meyer <i>et al.</i> ²⁵	$\text{Ba}_9\text{Ce}_6\text{Cl}_{34}\text{O}$	11.348(3)	21.729(5)	2798(2)

$x(\text{NdCl}_3) = 0.05$ and 0.25 (see Section 4.7.2) correspond to the formation event of a high-temperature solid solution.

Quenching experiments were performed at a temperature of 973 K, for compositions $0.1 \leq x(\text{NdCl}_3) \leq 0.3$. These experiments confirmed the existence of a solid solution, as the cell parameters of $(\text{Ba},\text{Nd})\text{Cl}_{2+x}$ decrease upon the addition of NdCl_3 . It is, however, not possible to quantify the extent of the solid solution at this temperature based on the present quenching experiments, due to the fact that the predicted stability range at 973 K is very narrow. Moreover, the experiments performed at $x(\text{NdCl}_3) = 0.1$ and 0.25 show additional phases, namely α - BaCl_2 and $\text{Ba}_3\text{Nd}_2\text{Cl}_{12}$ respectively, which is in agreement with the expected phases based on the phase diagram in Fig. 11. The profile refinement of the experiment performed at $x(\text{NdCl}_3) = 0.10$ is shown in Fig. 7 and shows the phases that were expected based on the phase diagram. The other profile refinements obtained from the post-XRD analyses are reported in the supplementary information to this work.

4.5. Solid-solutions – $\text{Nd}_y\text{AE}_{1-y}\text{Cl}_{3-y}$ (AE = Sr, Ba)

Quenching experiments and post-XRD were also carried out to investigate the solid solution on the NdCl_3 -rich side of the SrCl_2 – NdCl_3 system. The calculated cell volume is slightly larger than that of NdCl_3 , as expected from the respective crystal radii ($r_{\text{Nd}(3+),\text{VI}} = 1.123$ Å, $r_{\text{Sr}(2+),\text{VI}} = 1.32$ Å²⁹), but the difference is within the margin of experimental error.

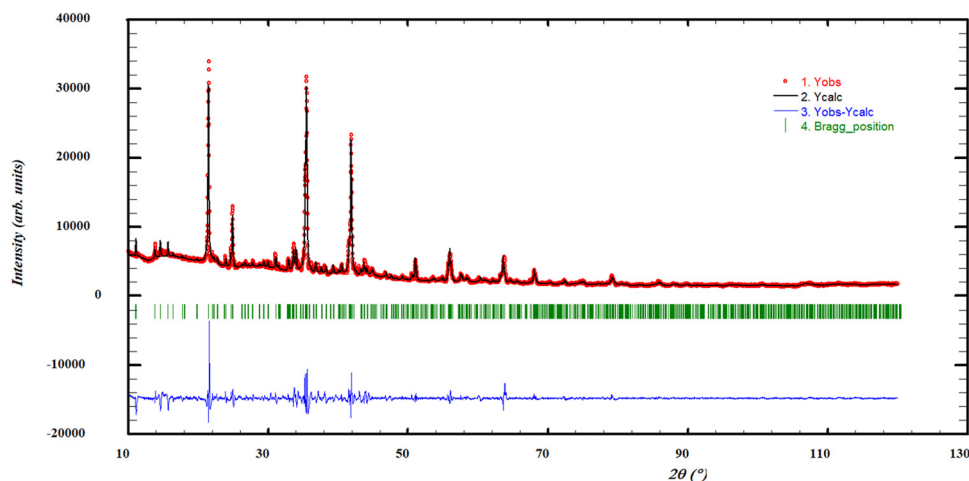


Fig. 3 Profile refinement of the intermediate salt $\text{Ba}_3\text{Nd}_2\text{Cl}_{12}$, using the structure of $\text{Ba}_9\text{Nd}_6\text{Cl}_{34}\text{O}$ as reported by Meyer *et al.* as crystal structure. The observed intensity (Y_{obs} , red) is plotted along with the calculated intensity from the refinement (Y_{calc} , black), and the difference between the two is shown ($Y_{\text{obs}} - Y_{\text{calc}}$, blue). The angles at which reflections occur are shown as well (Bragg positions, vertical lines). Measurement at $\lambda = \text{Cu-K}\alpha$.



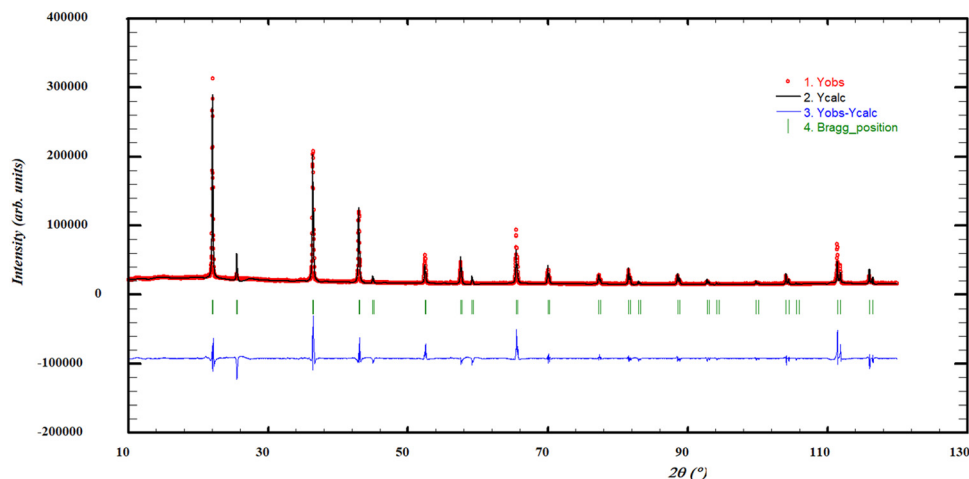


Fig. 4 Profile refinement of a quenched sample with $x(\text{NdCl}_3) = 0.1$, showing solid solution $\text{Sr}_{1-x}\text{Nd}_x\text{Cl}_{2+x}$, quenched from 850 K. The observed intensity (Y_{obs} , red) is plotted along with the calculated intensity from the refinement (Y_{calc} , black), and the difference between the two is shown ($Y_{\text{obs}} - Y_{\text{calc}}$, blue). The angles at which reflections occur are shown as well (Bragg positions, vertical lines). Measured at $\lambda = \text{Cu-K}\alpha$.

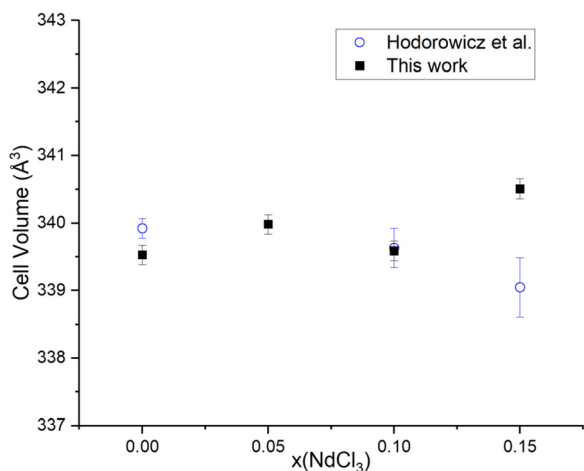


Fig. 5 Cell volumes of the cubic $\text{Sr}_{1-x}\text{Nd}_x\text{Cl}_{2+x}$ (space group $Fm\bar{3}m$) phase, calculated from the profile refinements of the solid solutions quenched in the $\text{SrCl}_2\text{--NdCl}_3$ system for $T = 923$ K.

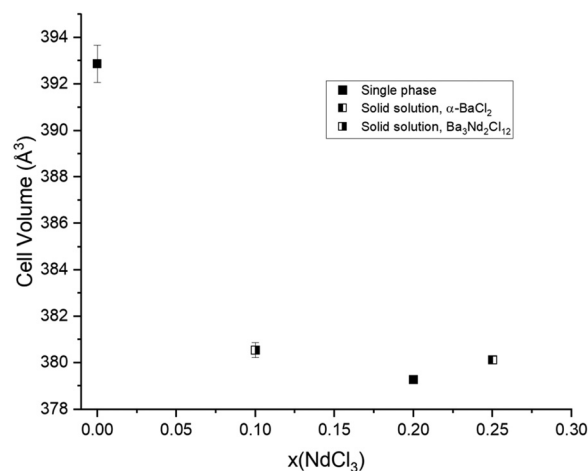


Fig. 6 Cell volumes of the cubic $\text{Ba}_{1-x}\text{Nd}_x\text{Cl}_{2+x}$ phase, calculated from the profile refinements of the quenching experiments performed in the $\text{BaCl}_2\text{--NdCl}_3$ system at $T = 973$ K.

No quenching experiments were carried out to investigate the existence of a solid solution on the NdCl_3 -rich side of the $\text{BaCl}_2\text{--NdCl}_3$ phase diagram. However, a small decrease of the eutectic temperature at $x(\text{NdCl}_3) = 0.948$ and 0.969 is observed, consistent with the formation of a solid solution in this composition range. This is also consistent with the observations of Alders *et al.*¹⁶ in their work on the $\text{BaCl}_2\text{--CeCl}_3$ system. The existence of solid solutions at the NdCl_3 -rich side of the $\text{AECl}_2\text{--NdCl}_3$ ($\text{AE} = \text{Sr}, \text{Ba}$) systems is also supported by the Tamman-diagrams in Fig. 10 and 13, respectively (see Sections 4.7.1 and 4.7.2).

4.6. Phase equilibria measurements

A list of mixtures measured in this work by DSC, along with the temperatures of invariant transitions and associated invariant

reactions, is presented in Tables 5 and 6 for the $\text{SrCl}_2\text{--NdCl}_3$ and $\text{BaCl}_2\text{--NdCl}_3$ systems, respectively. The phase equilibria are also shown on the optimized phase diagrams in Fig. 8 and 11, respectively.

4.7. Thermodynamic models

4.7.1. $\text{SrCl}_2\text{--NdCl}_3$. With the thermodynamic descriptions of the parameters in the system as described in eqn (1), (7) and (15), the phase diagram and mixing enthalpy of the system were calculated. The optimized phase diagram is shown in Fig. 8, and the enthalpy of mixing is reported in Fig. 9. The invariant equilibria calculated with this CALPHAD model are presented, and compared with the available experimental data in Table 7.

The CALPHAD model presented in Fig. 8 was optimized to fit the experimental data obtained in this work by DSC. There is, however, a significant discrepancy between the calculated



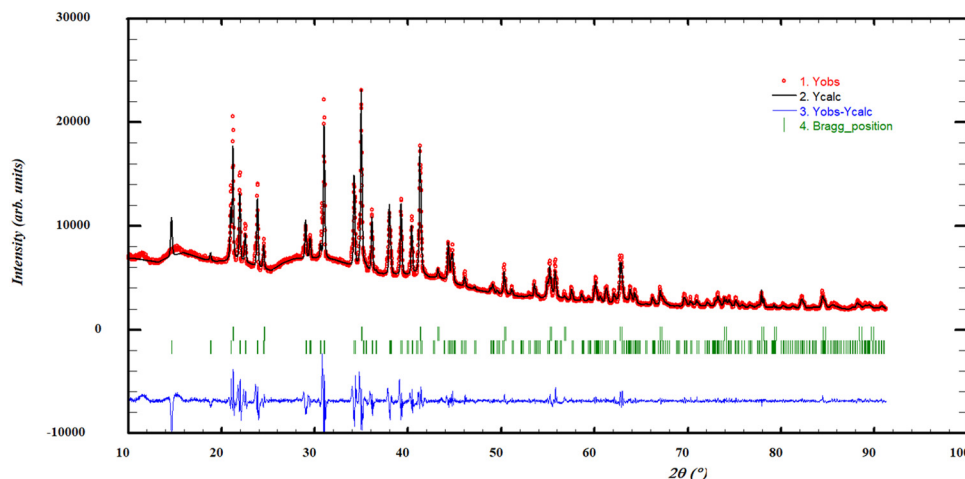


Fig. 7 Profile refinement of a quenched sample with $x(\text{NdCl}_3) = 0.10$, showing both the solid solution $\text{Ba}_{1-x}\text{Nd}_x\text{Cl}_{2+x}$ and $\alpha\text{-BaCl}_2$, quenched from 973 K. The observed intensity (Y_{obs} , red) is plotted along with the calculated intensity from the refinement (Y_{calc} , black), and the difference between the two is shown ($Y_{\text{obs}} - Y_{\text{calc}}$, blue). The angles at which reflections occur are shown as well (Bragg positions, vertical lines). Measured at $\lambda = \text{Cu-K}\alpha$.

Table 5 Equilibrium data in the $\text{SrCl}_2\text{-NdCl}_3$ system as measured by DSC

x_{NdCl_3} ^a	T^b (K)	Equilibrium	Equilibrium reaction
0	1147	Congruent melting	$\text{SrCl}_2 = \text{L}$
0.100	1123	Liquidus	$\text{Sr}_{1-x}\text{Nd}_x\text{Cl}_{2+x} + \text{L}' = \text{L}$
0.150	1104	Liquidus	$\text{Sr}_{1-x}\text{Nd}_x\text{Cl}_{2+x} + \text{L}' = \text{L}$
0.203	1075	Liquidus	$\text{Sr}_{1-x}\text{Nd}_x\text{Cl}_{2+x} + \text{L}' = \text{L}$
0.229	1064	Liquidus	$\text{Sr}_{1-x}\text{Nd}_x\text{Cl}_{2+x} + \text{L}' = \text{L}$
	897	Peritectic	$\text{Sr}_9\text{Nd}_5\text{Cl}_{33} = \text{Sr}_{1-x}\text{Nd}_x\text{Cl}_{2+x} + \text{L}'$
0.251	1045	Liquidus	$\text{Sr}_{1-x}\text{Nd}_x\text{Cl}_{2+x} + \text{L}' = \text{L}$
	883	Peritectic	$\text{Sr}_9\text{Nd}_5\text{Cl}_{33} = \text{Sr}_{1-x}\text{Nd}_x\text{Cl}_{2+x} + \text{L}'$
0.269	1037	Liquidus	$\text{Sr}_{1-x}\text{Nd}_x\text{Cl}_{2+x} + \text{L}' = \text{L}$
	894	Peritectic	$\text{Sr}_9\text{Nd}_5\text{Cl}_{33} = \text{Sr}_{1-x}\text{Nd}_x\text{Cl}_{2+x} + \text{L}'$
0.359	981	Liquidus	$\text{Sr}_{1-x}\text{Nd}_x\text{Cl}_{2+x} + \text{L}' = \text{L}$
	894	Peritectic	$\text{Sr}_9\text{Nd}_5\text{Cl}_{33} = \text{Sr}_{1-x}\text{Nd}_x\text{Cl}_{2+x} + \text{L}'$
	872	Eutectic	$\text{Sr}_9\text{Nd}_5\text{Cl}_{33} + \text{Nd}_{1-y}\text{Sr}_y\text{Cl}_{3-y} = \text{L}$
0.449	910	Liquidus	$\text{Sr}_{1-x}\text{Nd}_x\text{Cl}_{2+x} + \text{L}' = \text{L}$
	883	Peritectic	$\text{Sr}_9\text{Nd}_5\text{Cl}_{33} = \text{Sr}_{1-x}\text{Nd}_x\text{Cl}_{2+x} + \text{L}'$
	874	Eutectic	$\text{Sr}_9\text{Nd}_5\text{Cl}_{33} + \text{Nd}_{1-y}\text{Sr}_y\text{Cl}_{3-y} = \text{L}$
0.530	885	Eutectic	$\text{Sr}_9\text{Nd}_5\text{Cl}_{33} + \text{Nd}_{1-y}\text{Sr}_y\text{Cl}_{3-y} = \text{L}$
0.570	873	Eutectic	$\text{Sr}_9\text{Nd}_5\text{Cl}_{33} + \text{Nd}_{1-y}\text{Sr}_y\text{Cl}_{3-y} = \text{L}$
0.599	919	Liquidus	$\text{Nd}_{1-y}\text{Sr}_y\text{Cl}_{3-y} + \text{L}' = \text{L}$
	874	Eutectic	$\text{Sr}_9\text{Nd}_5\text{Cl}_{33} + \text{Nd}_{1-y}\text{Sr}_y\text{Cl}_{3-y} = \text{L}$
0.699	955	Liquidus	$\text{Nd}_{1-y}\text{Sr}_y\text{Cl}_{3-y} + \text{L}' = \text{L}$
	875	Eutectic	$\text{Sr}_9\text{Nd}_5\text{Cl}_{33} + \text{Nd}_{1-y}\text{Sr}_y\text{Cl}_{3-y} = \text{L}$
0.899	1009	Liquidus	$\text{Nd}_{1-y}\text{Sr}_y\text{Cl}_{3-y} + \text{L}' = \text{L}$
	874	Eutectic	$\text{Sr}_9\text{Nd}_5\text{Cl}_{33} + \text{Nd}_{1-y}\text{Sr}_y\text{Cl}_{3-y} = \text{L}$
0.948	1019	Liquidus	$\text{Nd}_{1-y}\text{Sr}_y\text{Cl}_{3-y} + \text{L}' = \text{L}$
	868	Eutectic	$\text{Sr}_9\text{Nd}_5\text{Cl}_{33} + \text{Nd}_{1-y}\text{Sr}_y\text{Cl}_{3-y} = \text{L}$
1	1031	Congruent melting	$\text{NdCl}_3 = \text{L}$

^a The uncertainties on compositions x_{NdCl_3} are ± 0.005 . ^b The uncertainties on temperatures are ± 5 K for pure end-members and ± 10 K for mixtures.

liquidus between $x(\text{NdCl}_3) = 0.2$ and $x(\text{NdCl}_3) = 0.6$ when comparing to the data from Morozov *et al.*²³ and Vogel *et al.*²⁴ Given the fact that the data from these sources are not in agreement with each other, and that the actual liquidus we measure is in between the reported sets of data, we are confident in the accuracy of our experimental measurements and model in this composition range. The calculated mixing enthalpy has been optimized to fit the estimation obtained

using Davis' method, as presented in Fig. 9. The temperature and composition of the eutectic is in good agreement with the values measured in this work by DSC, as well as the values of Morozov *et al.* The eutectic data from Vogel *et al.* deviate greatly from the other two sources, and give us reason to not retain their data. The eutectic composition calculated by the model is in good agreement with the predicted composition from the Tammann-diagram in Fig. 10, where the heat flow area of the eutectic transition is plotted against composition.

The composition of the intermediate that we identified is also different from that reported by Morozov *et al.* and Vogel *et al.* report, but its existence is supported by the XRD data obtained in this work, as well as the work of Hodorowicz *et al.*²² It is also consistent with the limiting composition obtained at $x = 0.357$ in the Tammann diagram. The existence of mutual solid solubility of NdCl_3 and SrCl_2 was suggested previously by Vogel *et al.* and Hodorowicz *et al.*, which our data corroborate. Moreover, there is solubility of SrCl_2 in NdCl_3 up to 5% SrCl_2 at 900 K. This is again in line with the Tammann diagram in Fig. 10 where the area of the eutectic peak goes to zero at approximately $x(\text{NdCl}_3) = 0.95$, indicating that there is a solid solution at higher compositions.

4.7.2. $\text{BaCl}_2\text{-NdCl}_3$. With the optimized parameters as described in Table 1 and eqn (8) and (13), the phase diagram and mixing enthalpy of the system were calculated. The phase diagram is shown in Fig. 11, and the enthalpy of mixing is reported in Fig. 12. The invariant equilibria calculated with this CALPHAD model are presented and compared with the available experimental data in Table 8.

The CALPHAD model displayed in Fig. 11 was optimized to fit the measured invariant points, as well as the estimated mixing enthalpy as shown in Fig. 12. The DSC data between $0.05 \leq x(\text{NdCl}_3) \leq 0.3$ at $T = 935$ K that were not observed by Morozov *et al.*²³ or Vogel *et al.*²⁴ are explained rather well by the addition of a solid solution phase $\text{Ba}_{1-x}\text{Nd}_x\text{Cl}_{2+x}$, stable only at elevated temperatures. The temperature of the

Table 6 Equilibrium data in the BaCl₂–NdCl₃ system as measured by DSC

$x_{\text{NdCl}_3}^a$	T^b (K)	Equilibrium	Equilibrium reaction
0	1235	Congruent melting	$\beta\text{-BaCl}_2 = \text{L}$
	1198	α – β transition	$\alpha\text{-BaCl}_2 = \beta\text{-BaCl}_2$
0.06	1234	Liquidus	$\text{Ba}_{1-x}\text{Nd}_x\text{Cl}_{2+x} + \text{L}' = \text{L}$
	1134	Solidus	$\alpha\text{-BaCl}_2 + \text{Ba}_{1-x}\text{Nd}_x\text{Cl}_{2+x} = \text{Ba}_{1-x}\text{Nd}_x\text{Cl}_{2+x}$
	941	Eutectoid	$\alpha\text{-BaCl}_2 + \text{Ba}_3\text{Nd}_2\text{Cl}_{12} = \text{Ba}_{1-x}\text{Nd}_x\text{Cl}_{2+x}$
0.148	1202	Liquidus	$\text{Ba}_{1-x}\text{Nd}_x\text{Cl}_{2+x} + \text{L}' = \text{L}$
	939	Eutectoid	$\alpha\text{-BaCl}_2 + \text{Ba}_3\text{Nd}_2\text{Cl}_{12} = \text{Ba}_{1-x}\text{Nd}_x\text{Cl}_{2+x}$
0.207	1172	Liquidus	$\text{Ba}_{1-x}\text{Nd}_x\text{Cl}_{2+x} + \text{L}' = \text{L}$
	1020	Peritectic	$\text{Ba}_3\text{Nd}_2\text{Cl}_{12} = \text{Ba}_{1-x}\text{Nd}_x\text{Cl}_{2+x} + \text{L}'$
	939	Eutectoid	$\alpha\text{-BaCl}_2 + \text{Ba}_3\text{Nd}_2\text{Cl}_{12} = \text{Ba}_{1-x}\text{Nd}_x\text{Cl}_{2+x}$
0.249	1153	Liquidus	$\text{Ba}_{1-x}\text{Nd}_x\text{Cl}_{2+x} + \text{L}' = \text{L}$
	1023	Peritectic	$\text{Ba}_3\text{Nd}_2\text{Cl}_{12} = \text{Ba}_{1-x}\text{Nd}_x\text{Cl}_{2+x} + \text{L}'$
	939	Eutectoid	$\alpha\text{-BaCl}_2 + \text{Ba}_3\text{Nd}_2\text{Cl}_{12} = \text{Ba}_{1-x}\text{Nd}_x\text{Cl}_{2+x}$
0.265	1132	Liquidus	$\text{Ba}_{1-x}\text{Nd}_x\text{Cl}_{2+x} + \text{L}' = \text{L}$
	1024	Peritectic	$\text{Ba}_3\text{Nd}_2\text{Cl}_{12} = \text{Ba}_{1-x}\text{Nd}_x\text{Cl}_{2+x} + \text{L}'$
	938	Eutectoid	$\alpha\text{-BaCl}_2 + \text{Ba}_3\text{Nd}_2\text{Cl}_{12} = \text{Ba}_{1-x}\text{Nd}_x\text{Cl}_{2+x}$
0.305	1113	Liquidus	$\text{Ba}_{1-x}\text{Nd}_x\text{Cl}_{2+x} + \text{L}' = \text{L}$
	1031	Peritectic	$\text{Ba}_3\text{Nd}_2\text{Cl}_{12} = \text{Ba}_{1-x}\text{Nd}_x\text{Cl}_{2+x} + \text{L}'$
0.370	1045	Liquidus	$\text{Ba}_{1-x}\text{Nd}_x\text{Cl}_{2+x} + \text{L}' = \text{L}$
	1018	Peritectic	$\text{Ba}_3\text{Nd}_2\text{Cl}_{12} = \text{Ba}_{1-x}\text{Nd}_x\text{Cl}_{2+x} + \text{L}'$
0.380	1043	Liquidus	$\text{Ba}_{1-x}\text{Nd}_x\text{Cl}_{2+x} + \text{L}' = \text{L}$
	1017	Peritectic	$\text{Ba}_3\text{Nd}_2\text{Cl}_{12} = \text{Ba}_{1-x}\text{Nd}_x\text{Cl}_{2+x} + \text{L}'$
0.391	1039	Liquidus	$\text{Ba}_{1-x}\text{Nd}_x\text{Cl}_{2+x} + \text{L}' = \text{L}$
	1019	Peritectic	$\text{Ba}_3\text{Nd}_2\text{Cl}_{12} = \text{Ba}_{1-x}\text{Nd}_x\text{Cl}_{2+x} + \text{L}'$
	893	Eutectic	$\text{Ba}_3\text{Nd}_2\text{Cl}_{12} + \text{Nd}_{1-y}\text{Ba}_y\text{Cl}_{3-y} = \text{L}$
0.405	1035	Liquidus	$\text{Ba}_{1-x}\text{Nd}_x\text{Cl}_{2+x} + \text{L}' = \text{L}$
	1015	Peritectic	$\text{Ba}_3\text{Nd}_2\text{Cl}_{12} = \text{Ba}_{1-x}\text{Nd}_x\text{Cl}_{2+x} + \text{L}'$
	894	Eutectic	$\text{Ba}_3\text{Nd}_2\text{Cl}_{12} + \text{Nd}_{1-y}\text{Ba}_y\text{Cl}_{3-y} = \text{L}$
0.41	1018	Peritectic	$\text{Ba}_3\text{Nd}_2\text{Cl}_{12} = \text{Ba}_{1-x}\text{Nd}_x\text{Cl}_{2+x} + \text{L}'$
	908	Eutectic	$\text{Ba}_3\text{Nd}_2\text{Cl}_{12} + \text{Nd}_{1-y}\text{Ba}_y\text{Cl}_{3-y} = \text{L}$
0.431	896	Eutectic	$\text{Ba}_3\text{Nd}_2\text{Cl}_{12} + \text{Nd}_{1-y}\text{Ba}_y\text{Cl}_{3-y} = \text{L}$
0.498	1010	Liquidus	$\text{Ba}_3\text{Nd}_2\text{Cl}_{12} + \text{L}' = \text{L}$
	910	Eutectic	$\text{Ba}_3\text{Nd}_2\text{Cl}_{12} + \text{Nd}_{1-y}\text{Ba}_y\text{Cl}_{3-y} = \text{L}$
0.55	989	Liquidus	$\text{Ba}_3\text{Nd}_2\text{Cl}_{12} + \text{L}' = \text{L}$
	912	Eutectic	$\text{Ba}_3\text{Nd}_2\text{Cl}_{12} + \text{Nd}_{1-y}\text{Ba}_y\text{Cl}_{3-y} = \text{L}$
0.600	924	Liquidus	$\text{Nd}_{1-y}\text{Ba}_y\text{Cl}_{3-y} + \text{L}' = \text{L}$
	899	Eutectic	$\text{Ba}_3\text{Nd}_2\text{Cl}_{12} + \text{Nd}_{1-y}\text{Ba}_y\text{Cl}_{3-y} = \text{L}$
0.674	912	Eutectic	$\text{Ba}_3\text{Nd}_2\text{Cl}_{12} + \text{Nd}_{1-y}\text{Ba}_y\text{Cl}_{3-y} = \text{L}$
0.753	962	Liquidus	$\text{Nd}_{1-y}\text{Ba}_y\text{Cl}_{3-y} + \text{L}' = \text{L}$
	902	Eutectic	$\text{Ba}_3\text{Nd}_2\text{Cl}_{12} + \text{Nd}_{1-y}\text{Ba}_y\text{Cl}_{3-y} = \text{L}$
0.850	1000	Liquidus	$\text{Nd}_{1-y}\text{Ba}_y\text{Cl}_{3-y} + \text{L}' = \text{L}$
	915	Eutectic	$\text{Ba}_3\text{Nd}_2\text{Cl}_{12} + \text{Nd}_{1-y}\text{Ba}_y\text{Cl}_{3-y} = \text{L}$
	899	Unknown	—
0.948	1026	Liquidus	$\text{Nd}_{1-y}\text{Ba}_y\text{Cl}_{3-y} + \text{L}' = \text{L}$
	904	Eutectic	$\text{Nd}_{1-y}\text{Ba}_y\text{Cl}_{3-y} = \text{L}$
	897	Solidus	$\text{Ba}_3\text{Nd}_2\text{Cl}_{12} + \text{Nd}_{1-y}\text{Ba}_y\text{Cl}_{3-y} = \text{Nd}_{1-y}\text{Ba}_y\text{Cl}_{3-y}$
0.969	1030	Liquidus	$\text{Nd}_{1-y}\text{Ba}_y\text{Cl}_{3-y} + \text{L}' = \text{L}$
	970	Solidus	$\text{Nd}_{1-y}\text{Ba}_y\text{Cl}_{3-y} = \text{Nd}_{1-y}\text{Ba}_y\text{Cl}_{3-y} + \text{L}'$
	894	Solidus	$\text{Ba}_3\text{Nd}_2\text{Cl}_{12} + \text{Nd}_{1-y}\text{Ba}_y\text{Cl}_{3-y} = \text{Nd}_{1-y}\text{Ba}_y\text{Cl}_{3-y}$

^a The uncertainties on compositions x_{NdCl_3} are ± 0.005 . ^b The uncertainties on temperatures are ± 5 K for pure end-members and ± 10 K for mixtures.

peritectic, as well as the temperature and composition of the eutectic, are reproduced accurately by the model. While both Morozov *et al.* and Vogel *et al.* reported an intermediate of composition Ba₃NdCl₉ to be stable in this system, the absence of a eutectic event at compositions $x(\text{NdCl}_3) \leq 0.39$ indicates that the intermediate Ba₃Nd₂Cl₁₂ is more likely, as is corroborated by the XRD analysis presented in this work, and the limiting composition of $x = 0.4$ in the Tammann diagram, as seen in Fig. 13.

There is good agreement between the literature and our experimental data on the temperatures of the eutectic and peritectic equilibria, as seen in Table 8, as well as with the Tammann diagram presented in Fig. 13, which shows the recorded heat flow

area of the eutectic transition *versus* temperature. Solid solubility of NdCl₃ in BaCl₂ was already suggested by Vogel *et al.*, and the data in the Tammann diagram in Fig. 13 indicate that there is a narrow solid solution on the NdCl₃-rich side as well, with a limiting composition of 96% NdCl₃.

To further cement the potential of neodymium as a simulant for plutonium in the context of molten chlorides, a comparison is drawn between the systems AECl₂–NdCl₃ (AE = Sr, Ba) and the corresponding AECl₂–PuCl₃ system. In the case of the BaCl₂–PuCl₃ system, the model from our previous work on the BaCl₂–CeCl₃ system is included in the comparison.

As seen in Fig. 14, the liquidus line and eutectic of the SrCl₂–PuCl₃ system is approximated very well by the thermodynamic



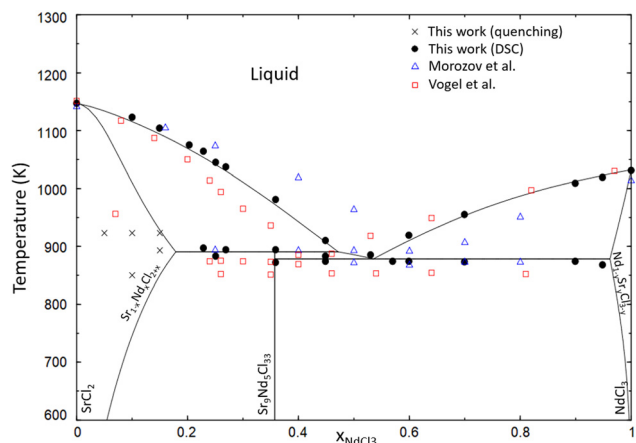


Fig. 8 Phase diagram of the SrCl_2 - NdCl_3 binary system, as calculated with the optimized thermodynamic model. Data from Morozov *et al.*²³ (empty blue triangles), Vogel *et al.*²⁴ (empty red squares) and this work (filled black circles). The compositions and temperatures at which quenching experiments have been performed are marked with black crosses.

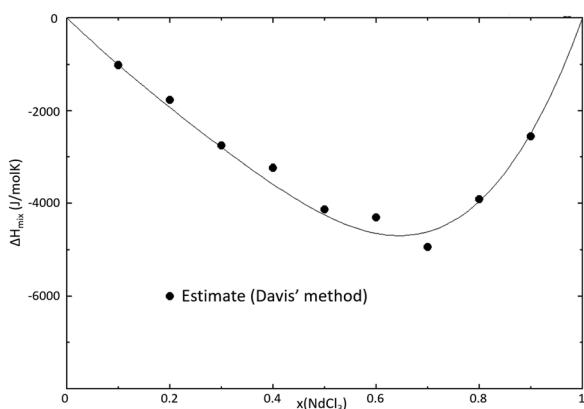


Fig. 9 Mixing enthalpy of the SrCl_2 - NdCl_3 binary system at $T = 1273$ K, as calculated with the thermodynamic model. The mixing enthalpy data were obtained with the mixing enthalpy estimation method presented by Davis and Rice,²¹ highlighted in a previous work.¹⁶

model of the SrCl_2 - NdCl_3 system. The comparison of the BaCl_2 - MCl_3 systems shown in Fig. 15 shows that the liquidus line of the PuCl_3 -system is very similar to the one calculated with the model of the BaCl_2 - NdCl_3 system, and that it deviates slightly from the CeCl_3 -system, owing to the higher melting point of CeCl_3 . Fig. 14 and 15 both show that, like in the

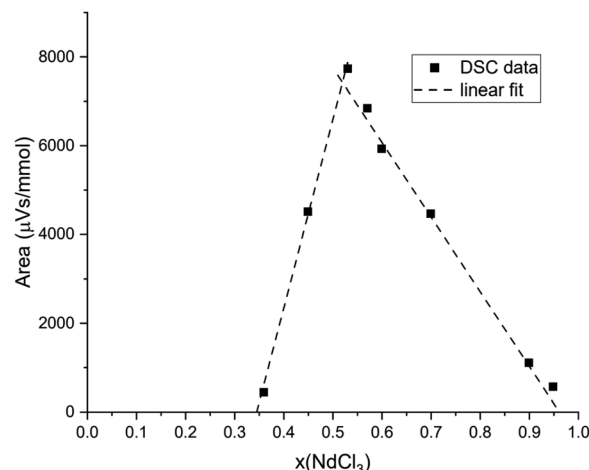


Fig. 10 Tammann-diagram showing the heat flow area of the eutectic transition versus composition, obtained in this work on the SrCl_2 - NdCl_3 system. The intersection of the linear fits (dashed lines) is the predicted composition of the eutectic in this system, and the diagram matches with the composition of the intermediate.

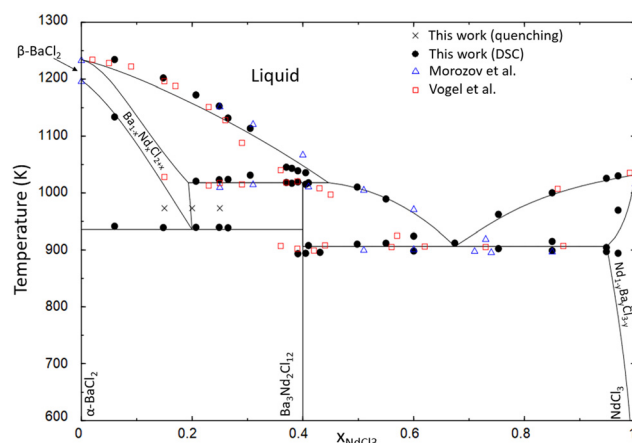


Fig. 11 Phase diagram of the BaCl_2 - NdCl_3 binary system, as calculated with the optimized thermodynamic model. Data from Morozov *et al.*²³ (empty blue triangles), Vogel *et al.*²⁴ (empty red squares) and this work (filled black circles). The compositions and temperatures at which quenching experiments have been performed are marked with black crosses.

systems NaCl - MCl_3 shown in Section 4.1, neodymium is a very accurate simulant for the melting behaviour of plutonium in molten chlorides.

Table 7 Calculated invariant equilibria in the SrCl_2 - NdCl_3 system, as well as experimentally measured values of these invariants from Morozov *et al.*²³ Vogel *et al.*²⁴ and this work (DSC). The numbers in parentheses are the respective compositions of the eutectic

x_{NdCl_3}	T (K)				Equilibrium	Invariant reaction
	CALPHAD	Morozov <i>et al.</i> ²³	Vogel <i>et al.</i> ²⁴	This work (DSC)		
0	1146	1142	1151	1147 ± 5	Congruent melting	$\text{SrCl}_2 = \text{L}$
0.357	890	893	873	894 ± 10	Peritectic	$\text{Sr}_9\text{Nd}_5\text{Cl}_{33} = \text{Sr}_{1-x}\text{Nd}_x\text{Cl}_{2+x} + \text{L}'$
0.535	878 (0.530)	872 (0.560)	853 (0.420)	885 ± 10 (0.535)	Eutectic	$\text{Sr}_9\text{Nd}_5\text{Cl}_{33} + \text{Nd}_{1-y}\text{Sr}_y\text{Cl}_{3-y} = \text{L}$
1	1030	1016	—	1031 ± 5	Congruent melting	$\text{NdCl}_3 = \text{L}$

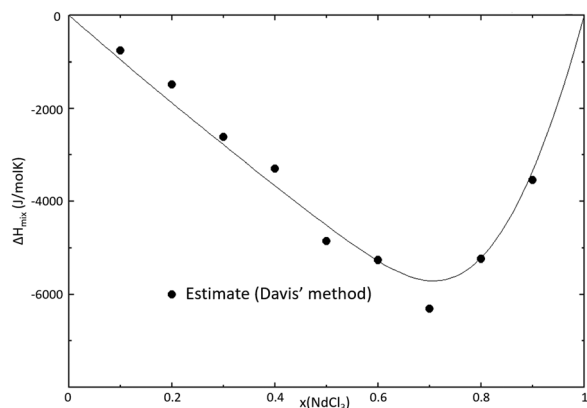


Fig. 12 Mixing enthalpy of the $\text{BaCl}_2\text{--NdCl}_3$ binary system at $T = 1273\text{ K}$, as calculated with the thermodynamic model presented in this section. The mixing enthalpy data were obtained with the mixing enthalpy estimation method presented by Davis and Rice,²¹ highlighted in a previous work.¹⁶

4.8. Ternary systems $\text{NaCl--SrCl}_2\text{--NdCl}_3$ and $\text{NaCl--BaCl}_2\text{--NdCl}_3$

Neodymium is a good candidate to act as a simulant for plutonium in chloride systems due to its similar melting behaviour and structural properties, the former being exemplified by the very similar liquidus equilibria in the NaCl--NdCl_3 and NaCl--PuCl_3 systems shown in Section 4.1. We believe that the investigations of the $\text{SrCl}_2\text{--NdCl}_3$ and $\text{BaCl}_2\text{--NdCl}_3$ systems as presented in this work can give valuable insights into the liquidus equilibria of the $\text{SrCl}_2\text{--PuCl}_3$ and $\text{BaCl}_2\text{--PuCl}_3$ systems too, which are more challenging to investigate experimentally. Moreover, they can be used to predict the melting behaviour of the molten salt fuel NaCl--PuCl_3 (some MSR designs rely on using the eutectic composition of this system) upon addition of the fission products Sr and Ba. To this end, thermodynamic calculations were performed in the ternary systems $\text{NaCl--SrCl}_2\text{--NdCl}_3$ and $\text{NaCl--BaCl}_2\text{--NdCl}_3$ as simulant systems to the equivalent PuCl_3 -based systems. For this, the binary subsystems NaCl--SrCl_2 , NaCl--BaCl_2 and NaCl--NdCl_3 were also modelled, which is presented in 7. The extrapolation to the ternary system is solely based on the constituting binary systems, and no ternary excess terms were added. The liquidus projections of these ternary systems are shown in Appendix C.

Fig. 16 shows the pseudo-binary phase diagram $\{0.95 (\text{NaCl} + \text{NdCl}_3) + 0.05\text{SrCl}_2\}$, and Fig. 17 shows the pseudo-binary

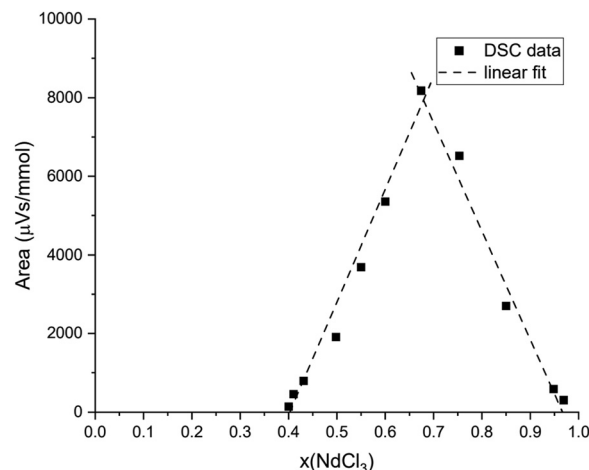


Fig. 13 Tammann-diagram calculated from the DSC data obtained in this work on the $\text{BaCl}_2\text{--NdCl}_3$ system. The intersection of the linear fits (dashed lines) is the predicted composition of the eutectic in this system. The limiting compositions are $x = 0.4$ (intermediate $\text{Ba}_3\text{Nd}_2\text{Cl}_{12}$) and $x = 0.96$ (solid solution $\text{Nd}_{1-y}\text{Ba}_y\text{Cl}_{3-y}$).

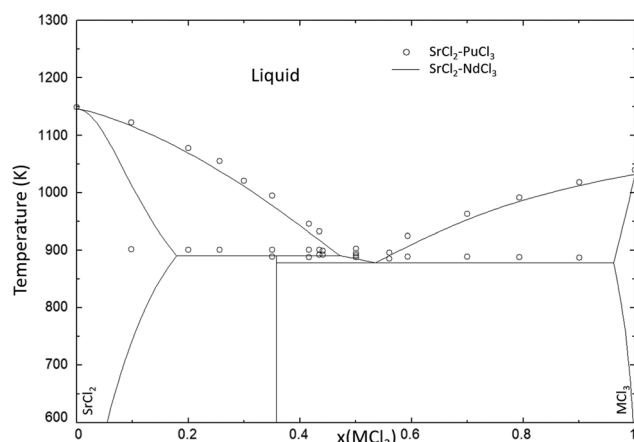


Fig. 14 Calculated phase diagram of the $\text{SrCl}_2\text{--NdCl}_3$ system (solid black line) compared to the experimental data on the $\text{SrCl}_2\text{--PuCl}_3$ (open black circles) system presented by Johnson *et al.*³⁰

phase diagram $\{0.95 (\text{NaCl} + \text{NdCl}_3) + 0.05\text{BaCl}_2\}$ to investigate the addition of 5% SrCl_2 or BaCl_2 to a NaCl--PuCl_3 mixture respectively. In this calculation, the addition of 5% fission product (Ba or Sr) is based on the order of magnitude of the

Table 8 Calculated invariant equilibria in the $\text{BaCl}_2\text{--NdCl}_3$ system, as well as experimentally measured values of these invariants from Morozov *et al.*,²³ Vogel *et al.*²⁴ and this work (DSC). The numbers in parentheses are the respective compositions of the eutectic

x_{NdCl_3}	$T\text{ (K)}$	CALPHAD	Morozov <i>et al.</i> ²³	Vogel <i>et al.</i> ²⁴	This work (DSC)	Equilibrium	Invariant reaction
0	1198	1200	1199	1197 ± 5		$\alpha\text{--}\beta$ transition	$\alpha\text{--BaCl}_2 = \beta\text{--BaCl}_2$
	1234	1243	1239	1235 ± 5		Congruent melting	$\beta\text{--BaCl}_2 = \text{L}$
0.2	935			939 ± 10		Eutectoid	$\alpha\text{--BaCl}_2 + \text{Ba}_3\text{Nd}_2\text{Cl}_{12} = \text{Ba}_{1-x}\text{Nd}_x\text{Cl}_{2+x}$
0.4	1017	1011	1020	1015 ± 10		Peritectic	$\text{Ba}_3\text{Nd}_2\text{Cl}_{12} = \text{Ba}_{1-x}\text{Nd}_x\text{Cl}_{2+x} + \text{L}'$
0.676	906 (0.676)	902 (0.710)	901 (0.620)	912 ± 10 (0.674)		Eutectic	$\text{Ba}_3\text{Nd}_2\text{Cl}_{12} + \text{Nd}_{1-y}\text{Ba}_y\text{Cl}_{3-y} = \text{L}$
1	1030	1016	—	1031 ± 5		Congruent melting	$\text{NdCl}_3 = \text{L}$

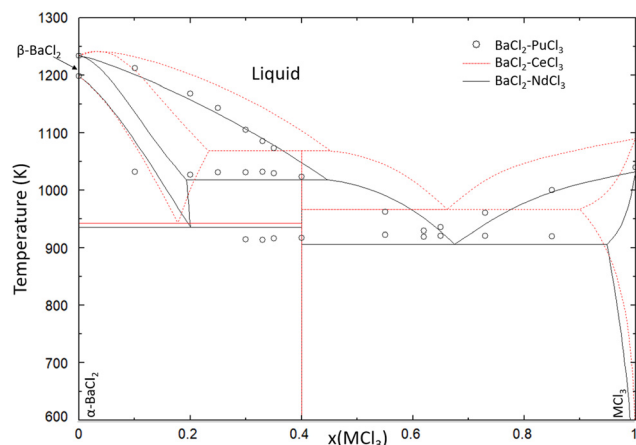


Fig. 15 Calculated phase diagram of the $\text{BaCl}_2\text{--NdCl}_3$ system (solid black line) compared to the model of $\text{BaCl}_2\text{--CeCl}_3$ from a previous work (dotted red line) and experimental data on the $\text{BaCl}_2\text{--PuCl}_3$ (open black circles) system presented by Johnson *et al.*³⁰

fission yield of Ba (9.5%) and Sr (5.48%).³¹ In an actual reactor operation scenario these percentages will be lower, as it is contingent upon the initial Pu-concentration. The observed effect of the addition of these fission products is therefore an amplification.

The calculated phase diagram in Fig. 16 shows that the addition of 5% SrCl_2 leads to a small decrease in the eutectic temperature (10 K). This indicates that the addition of the fission product Sr has no negative effect on the melting temperature of the fuel.

By contrast, the calculated phase diagram in Fig. 17 shows that the addition of 5% of BaCl_2 could cause the melting temperature of the eutectic to rise significantly. The primary

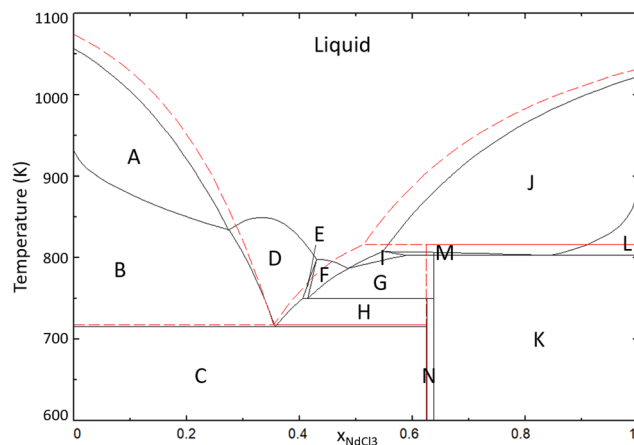


Fig. 17 Phase diagram of the $\{0.95\text{NaCl} + 0.05\text{BaCl}_2\}$ and $\{0.95\text{NdCl}_3 + 0.05\text{BaCl}_2\}$ pseudo-binary section of the $\text{NaCl}\text{--BaCl}_2\text{--NdCl}_3$ ternary system. The labelled phases are $\text{NaCl} + \text{L}'$ (A), $\text{NaCl} + \text{BaCl}_2 + \text{L}'$ (B), $\text{NaCl} + \text{BaCl}_2 + \text{Na}_3\text{Nd}_5\text{Cl}_{18}$ (C), $\text{BaCl}_2 + \text{L}'$ (D), $\text{BaCl}_2 + \text{Ba}_3\text{Nd}_2\text{Cl}_{12} + \text{L}'$ (E), $\text{Ba}_3\text{Nd}_2\text{Cl}_{12} + \text{L}'$ (F), $\text{Ba}_3\text{Nd}_2\text{Cl}_{12} + \text{Na}_3\text{Nd}_5\text{Cl}_{18} + \text{L}'$ (G), $\text{BaCl}_2 + \text{Na}_3\text{Nd}_5\text{Cl}_{18} + \text{L}'$ (H), $\text{Na}_3\text{Nd}_5\text{Cl}_{18} + \text{L}'$ (I), $\text{NdCl}_3 + \text{L}'$ (J), $\text{Ba}_3\text{Nd}_2\text{Cl}_{12} + \text{Na}_3\text{Nd}_5\text{Cl}_{18} + \text{Nd}_{1-y}\text{Ba}_y\text{Cl}_{3-y}$ (K), $\text{Ba}_3\text{Nd}_2\text{Cl}_{12} + \text{Nd}_{1-y}\text{Ba}_y\text{Cl}_{3-y} + \text{L}'$ (L), $\text{Na}_3\text{Nd}_5\text{Cl}_{18} + \text{Nd}_{1-y}\text{Ba}_y\text{Cl}_{3-y} + \text{L}'$ (M), $\text{Ba}_3\text{Nd}_2\text{Cl}_{12} + \text{Na}_3\text{Nd}_5\text{Cl}_{18} + \text{BaCl}_2$ (N). The lines in red correspond to the phase diagram of the system $\text{NaCl}\text{--NdCl}_3$.

crystallization phase above the eutectic composition of the $\text{NaCl}\text{--NdCl}_3$ system is BaCl_2 , indicating that BaCl_2 could precipitate out of the melt at high concentrations. This result would have significant consequences for the operation of the reactor, as the presence of precipitates could lead to clogging. This hypothesis should be assessed with experimental investigations and thorough modelling in the ternary system, including necessary ternary excess parameters.

5. Summary

Thermodynamic modelling assessments of the molten salt systems $\text{AECl}_2\text{--NdCl}_3$ ($\text{AE} = \text{Sr}, \text{Ba}$) are presented in this work using the CALPHAD method with the quasi-chemical formalism in quadruplet approximation for the liquid solution. The system $\text{SrCl}_2\text{--NdCl}_3$ is characterised by: (i) a single eutectic, (ii) a peritectic decomposition of the intermediate $\text{Sr}_9\text{Nd}_5\text{Cl}_{33}$, (iii) a $\text{Sr}_{1-x}\text{Nd}_x\text{Cl}_{2+x}$ (cubic) solid solution in the composition range $x(\text{NdCl}_3) = [0\text{--}0.2]$, (iv) a $\text{Nd}_{1-y}\text{Sr}_y\text{Cl}_{3-y}$ (hexagonal) solid solution in the composition range $x(\text{NdCl}_3) \geq 0.95$. The structure of the intermediate $\text{Sr}_9\text{Nd}_5\text{Cl}_{33}$ has been characterised with XRD, and the solid solution $\text{Sr}_{1-x}\text{Nd}_x\text{Cl}_{2+x}$ has been investigated with quenching experiments and post-XRD characterisation. Extrapolation to the ternary $\text{NaCl}\text{--SrCl}_2\text{--NdCl}_3$, used here as simulant for the $\text{NaCl}\text{--SrCl}_2\text{--PuCl}_3$ system, shows no adverse effects on the melting point of the eutectic upon addition of 5% SrCl_2 .

The system $\text{BaCl}_2\text{--NdCl}_3$ is similarly characterised by: (i) a single eutectic, (ii) a peritectic decomposition of the intermediate $\text{Ba}_3\text{Nd}_2\text{Cl}_{12}$, (iii) a $\text{Ba}_{1-x}\text{Nd}_x\text{Cl}_{2+x}$ (cubic) solid solution in the composition range $x(\text{NdCl}_3) = [0\text{--}0.2]$, stable only at temperatures above 940 K, (iv) a $\text{Nd}_{1-y}\text{Sr}_y\text{Cl}_{3-y}$ (hexagonal)

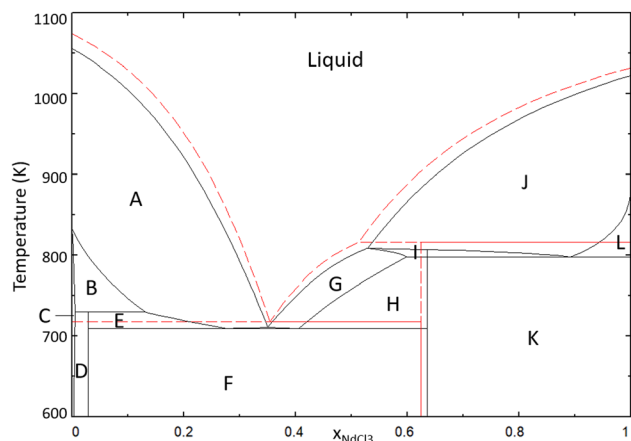


Fig. 16 Phase diagram of the $\{0.95\text{NaCl} + 0.05\text{SrCl}_2\}$ and $\{0.95\text{NdCl}_3 + 0.05\text{SrCl}_2\}$ pseudo-binary section of the $\text{NaCl}\text{--SrCl}_2\text{--NdCl}_3$ ternary system. The labelled phases are $\text{NaCl} + \text{L}'$ (A), $\text{NaCl} + \text{Sr}_{1-x}\text{Nd}_x\text{Cl}_{3-x} + \text{L}'$ (B), $\text{NaCl} + \text{Sr}_{1-x}\text{Nd}_x\text{Cl}_{3-x}$ (C), $\text{NaCl} + \text{Sr}_{1-x}\text{Nd}_x\text{Cl}_{3-x} + \text{Sr}_9\text{Nd}_5\text{Cl}_{33}$ (D), $\text{NaCl} + \text{Sr}_9\text{Nd}_5\text{Cl}_{33} + \text{L}'$ (E), $\text{NaCl} + \text{Sr}_9\text{Nd}_5\text{Cl}_{33} + \text{Na}_3\text{Nd}_5\text{Cl}_{18}$ (F), $\text{Na}_3\text{Nd}_5\text{Cl}_{18} + \text{L}'$ (G), $\text{Sr}_9\text{Nd}_5\text{Cl}_{33} + \text{Na}_3\text{Nd}_5\text{Cl}_{18} + \text{L}'$ (H), $\text{Na}_3\text{Nd}_5\text{Cl}_{18} + \text{Nd}_{1-y}\text{Sr}_y\text{Cl}_{2+y} + \text{L}'$ (I), $\text{Nd}_{1-y}\text{Sr}_y\text{Cl}_{2+y} + \text{L}'$ (J), $\text{Na}_3\text{Nd}_5\text{Cl}_{18} + \text{Nd}_{1-y}\text{Sr}_y\text{Cl}_{2+y} + \text{Sr}_9\text{Nd}_5\text{Cl}_{33}$ (K), $\text{Nd}_{1-y}\text{Sr}_y\text{Cl}_{2+y} + \text{Sr}_9\text{Nd}_5\text{Cl}_{33} + \text{L}'$ (L). The lines in red correspond to the phase diagram of the system $\text{NaCl}\text{--NdCl}_3$.



solid solution in the composition range $x(\text{NdCl}_3) \geq 0.95$. The structure of the intermediate $\text{Ba}_3\text{Nd}_2\text{Cl}_{12}$ has been determined using XRD, and the solid solution $\text{Ba}_{1-x}\text{Nd}_x\text{Cl}_{2+x}$ has been investigated with quenching experiments and post-XRD characterisation. Extrapolation to the ternary NaCl – BaCl_2 – NdCl_3 , used here as simulant for the NaCl – BaCl_2 – PuCl_3 system, shows that the addition of 5% BaCl_2 could potentially increase the melting point of the eutectic and lead to BaCl_2 precipitation in the melt. This would have implications for the safety assessment of the reactor, and should be confirmed in complementary investigations of the ternary system.

Data availability

Most of the experimental data obtained in this work has been reported in the main text in Tables 1–6 and Fig. 1–7, 9, 10, 12 and 13. Further supporting data have been included as part of the ESI.†

Conflicts of interest

The authors declare to have no competing financial interests or personal relationships that influence the work reported in this paper.

Appendices

Appendix A: thermodynamic functions SrCl_2

The end-member SrCl_2 undergoes a second order transition from a cubic structure, to a slightly distorted cubic structure in the temperature range 900–1100 K, as evidenced by the gradual bump in the enthalpy increment data of Dworkin and Bredig³² presented in Fig. 18. In previous works, such as that of Chartrand *et al.*,³³ this transition was incorporated in the model as a step-wise transition with an associated transition enthalpy of 6 kJ mol^{−1}. However, because this transition is not measured as an invariant equilibrium, in this work the α – β transition of SrCl_2 was not incorporated in the thermodynamic model. The thermodynamic functions from Chartrand *et al.*³³ were retained for the low-temperature α -phase, however.

Appendix B: modelling of binary systems with NaCl

In order to perform calculations in the ternary systems NaCl – SrCl_2 – NdCl_3 and NaCl – BaCl_2 – NdCl_3 , the binary systems NaCl – SrCl_2 , NaCl – BaCl_2 and NaCl – NdCl_3 were modelled based on the data presented in the literature. The cation–cation coordination numbers used in these models are the same as in Table 2, with the additional coordination numbers involving Na given in Table 9.

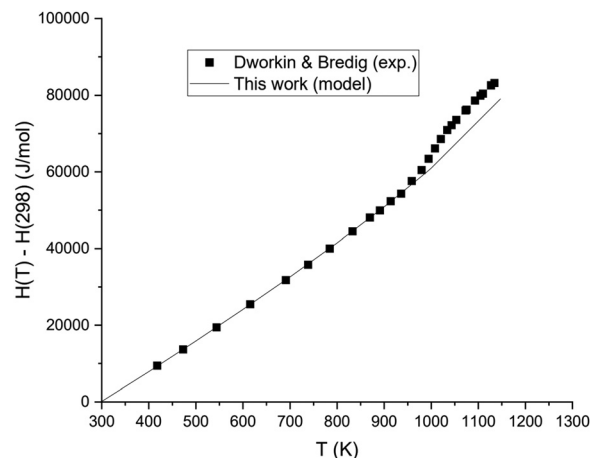


Fig. 18 Enthalpy increment data of SrCl_2 as measured experimentally by Dworkin and Bredig,³² compared to the calculated values using the thermodynamic functions from this work.

Table 9 Additional coordination numbers used in the CALPHAD models presented in this section

A	B	$Z_{AB/ClCl}^A$	$Z_{AB/ClCl}^B$	$Z_{AB/ClCl}^C$
Na	Na	6	6	6
Na	Nd	4	6	2.666
Na	Sr	3	6	3
Na	Ba	6	6	4

The thermodynamic model for the system NaCl – NdCl_3 was optimized using the phase diagram data presented by Sharma *et al.*³⁴ and Igarashi *et al.*³⁵ in the quadruplet approximation in the modified quasichemical formalism, as used throughout this work. The excess Gibbs energy function obtained through optimization of this binary is given in eqn (16), and the calculated phase diagram is shown in Fig. 19. The calculated mixing enthalpy is compared to experimental data in Fig. 20.

$$\Delta g_{\text{NaNd}/\text{ClCl}} = -9000 - 5.5T \quad (16)$$

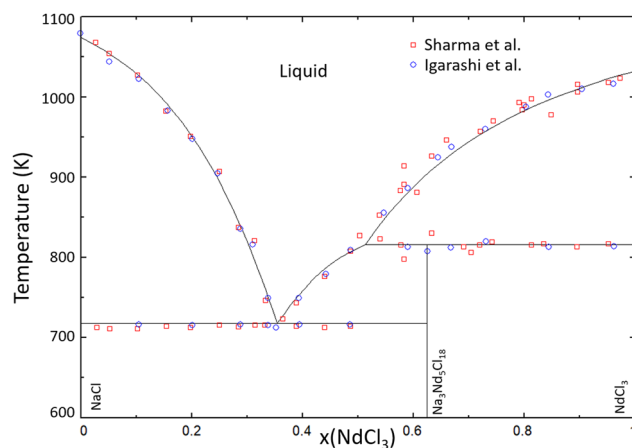


Fig. 19 Calculated phase diagram of the NaCl – NdCl_3 system modelled in this work. Experimental data were presented by Sharma *et al.*³⁴ (open red squares) and Igarashi *et al.*³⁵ (open blue circles).



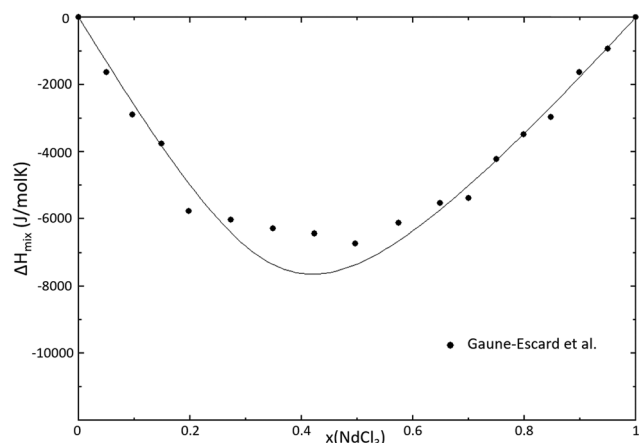


Fig. 20 Calculated mixing enthalpy of the NaCl–NdCl₃ system at $T = 1273$ K, modelled in this work. Experimental data were reported by Gaune-Escard *et al.*³⁶

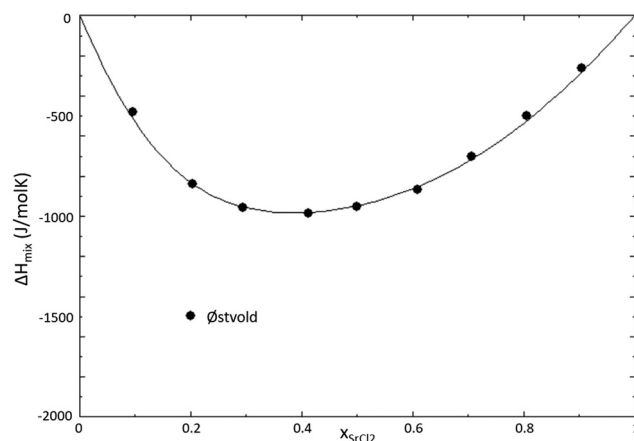


Fig. 22 Mixing enthalpy of the NaCl–SrCl₂ system calculated with the model presented in this work. Experimental data from Østvold *et al.*³⁶

The thermodynamic models for the NaCl–SrCl₂ and NaCl–BaCl₂ have already been presented by Chartrand *et al.*³³ However, since Chartrand *et al.* used different thermodynamic descriptions for the end-members, these systems were reassessed based on the experimental data available in the literature.

The system NaCl–SrCl₂ was optimized based on the experimentally determined phase diagram data by Vortisch *et al.*,³⁷ Scholich *et al.*³⁸ and Bukhalova *et al.*³⁹ The mixing enthalpy of the system was measured by Østvold *et al.*⁴⁰ The optimized phase diagram is shown in Fig. 21, and the calculated mixing enthalpy is given in Fig. 22. The excess Gibbs energy function is given in eqn (17).

$$\Delta g_{\text{NaSr/ClCl}} = -1119.3 + 0.4175T + \chi_{\text{NaSr/ClCl}}(-1067.8) + y_{\text{SrNa/ClCl}}(-996.4 + 1.3T) \quad (17)$$

The thermodynamic model of the NaCl–BaCl₂ system was optimized based on the experimental phase diagram data

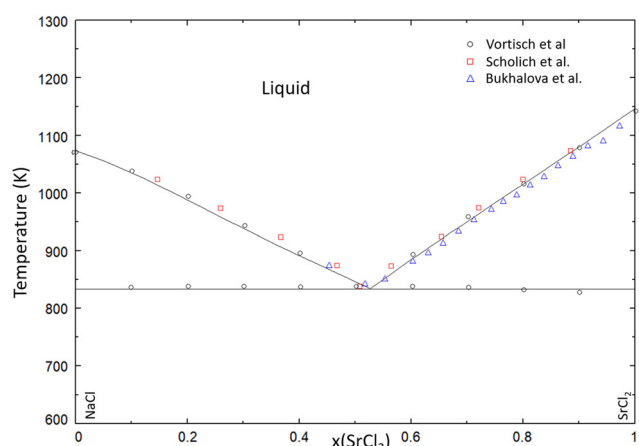


Fig. 21 Calculated phase diagram using the model presented in this work of the NaCl–SrCl₂ system. Experimental data from Vortisch *et al.*³⁷ (empty black circles), Scholich *et al.*³⁸ (empty red squares) and Bukhalova *et al.*³⁹ (empty blue triangles).

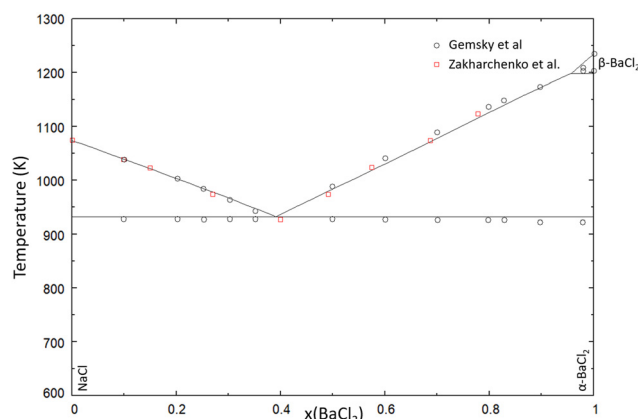


Fig. 23 Calculated phase diagram using the model presented in this work of the NaCl–BaCl₂ system. Experimental data from Gernsky *et al.*⁴¹ (empty black circles) and Zakharchenko *et al.*⁴² (empty red squares).

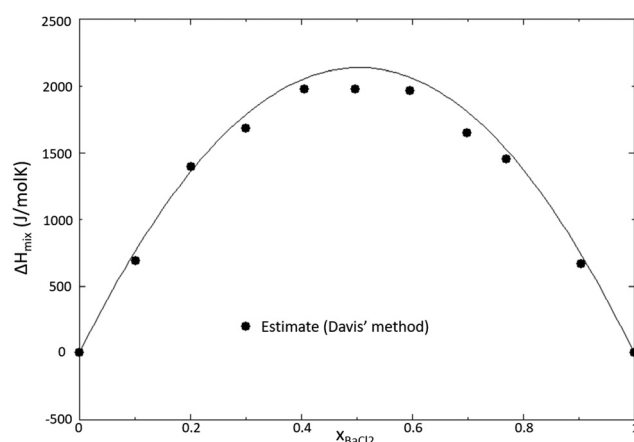


Fig. 24 Mixing enthalpy of the NaCl–BaCl₂ system calculated with the model presented in this work. Mixing enthalpy data estimated using the estimation method by Davis and Rice.²¹

presented by Gernsky *et al.*⁴¹ and Zakharchenko *et al.*⁴² No experimentally determined mixing enthalpy data are available



in the literature, and therefore the mixing enthalpy estimation method presented by Davis and Rice,²¹ also used for the systems SrCl₂-NdCl₃ and BaCl₂-NdCl₃ in this work, was used. The optimized phase diagram is shown in Fig. 23, and the calculated mixing enthalpy is shown in Fig. 24. The excess Gibbs energy function used in the model is given in eqn (18).

$$\Delta g_{\text{NaBa/ClCl}} = 2800 - 3T + y_{\text{BaNa/ClCl}}(-3T) \quad (18)$$

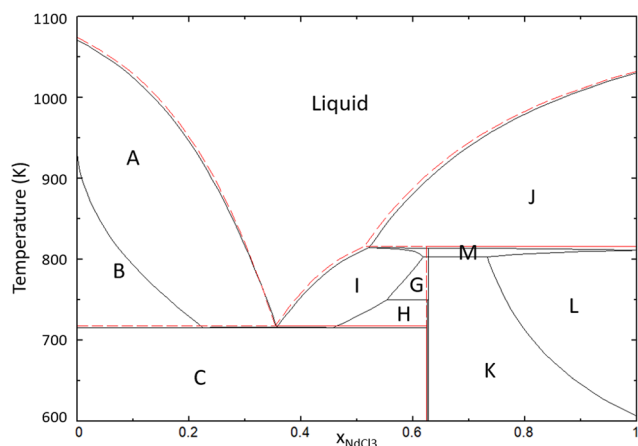


Fig. 25 Phase diagram of the {0.99NaCl + 0.01BaCl₂}–{0.99NdCl₃ + 0.01 BaCl₂} pseudo-binary system of the NaCl–BaCl₂–NdCl₃ ternary. The labelled phases are NaCl + L' (A), NaCl + BaCl₂ + L' (B), NaCl + BaCl₂ + Na₃Nd₅Cl₁₈ (C), Ba₃Nd₂Cl₁₂ + Na₃Nd₅Cl₁₈ + L' (G), BaCl₂ + Na₃Nd₅Cl₁₈ + L' (H), Na₃Nd₅Cl₁₈ + L' (I), NdCl₃ + L' (J), Ba₃Nd₂Cl₁₂ + Na₃Nd₅Cl₁₈ + Nd_{1-y}Ba₃Cl_{3-y} (K), Ba₃Nd₂Cl₁₂ + Nd_{1-y}Ba₃Cl_{3-y} + L' (L), Na₃Nd₅Cl₁₈ + Nd_{1-y}Ba₃Cl_{3-y} + L' (M).

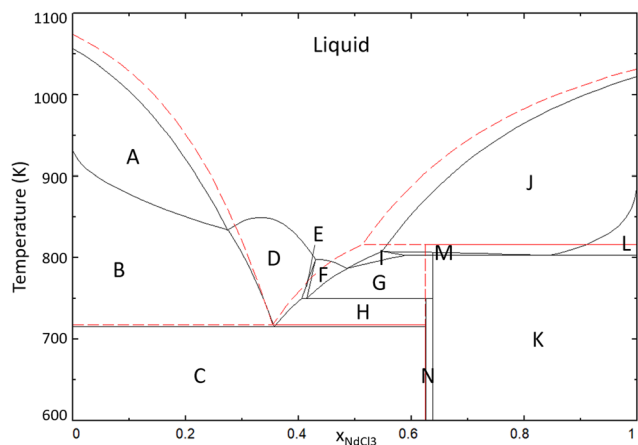


Fig. 26 Phase diagram of the {0.905NaCl + 0.095BaCl₂} and {0.905NdCl₃ + 0.095BaCl₂} pseudo-binary section of the NaCl–BaCl₂–NdCl₃ ternary system. The labelled phases are NaCl + L' (A), NaCl + BaCl₂ + L' (B), NaCl + BaCl₂ + Na₃Nd₅Cl₁₈ (C), BaCl₂ + L' (D), BaCl₂ + Ba₃Nd₂Cl₁₂ + L' (E), Ba₃Nd₂Cl₁₂ + L' (F), Ba₃Nd₂Cl₁₂ + Na₃Nd₅Cl₁₈ + L' (G), BaCl₂ + Na₃Nd₅Cl₁₈ + L' (H), Na₃Nd₅Cl₁₈ + L' (I), NdCl₃ + L' (J), Ba₃Nd₂Cl₁₂ + Na₃Nd₅Cl₁₈ + Nd_{1-y}Ba₃Cl_{3-y} (K), Ba₃Nd₂Cl₁₂ + Nd_{1-y}Ba₃Cl_{3-y} + L' (L), Ba₃Nd₂Cl₁₂ + Na₃Nd₅Cl₁₈ + BaCl₂ (N). The lines in red correspond to the phase diagram of the system NaCl–NdCl₃.

Appendix C: Ternary field investigations

In Section 4.8, the pseudo-binary systems {0.95NaCl + 0.05AECl₂}–{0.95NdCl₃ + 0.05AECl₂} (AE = Sr, Ba) have been presented, equivalent to the binary NaCl–NdCl₃ upon addition of 5% SrCl₂ or BaCl₂. The pseudo-binary phase diagram of NaCl–NdCl₃ upon addition of 1% and 9.5% BaCl₂ are presented here in Fig. 25 and 26 respectively. Fig. 27 and 28 show the projected liquidus surfaces of the ternary systems NaCl–SrCl₂–NdCl₃ and NaCl–BaCl₂–NdCl₃.

The liquidus projection of the NaCl–SrCl₂–NdCl₃ system shown in Fig. 27 indicates that the melting point of the eutectic of the NaCl–NdCl₃ binary is lowered slightly upon addition of small amounts of SrCl₂, as it approaches a ternary eutectic composition.

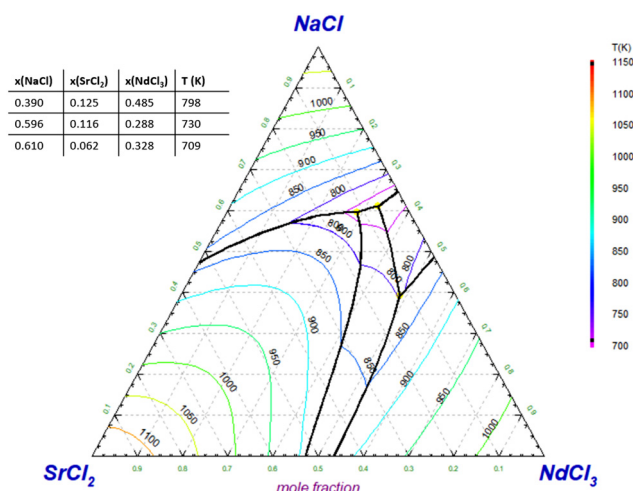


Fig. 27 Liquidus projection of the NaCl–SrCl₂–NdCl₃ system as calculated with the models presented in this work. No ternary excess terms were added.

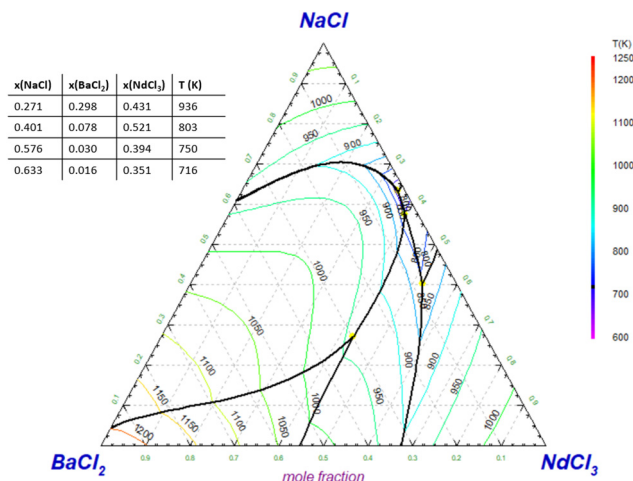


Fig. 28 Liquidus projection of the NaCl–BaCl₂–NdCl₃ system as calculated with the models presented in this work. No ternary excess terms were added.

Fig. 25 shows that the addition of 1% of BaCl_2 has no significant effect on the melting behaviour of the binary NaCl-NdCl_3 , with the eutectic being approximately the same as in the pure system. Upon further addition of BaCl_2 , as shown in Fig. 17 and 26, the eutectic temperature increases, and precipitation becomes more likely. The primary crystallization phase at the eutectic composition is BaCl_2 . The liquidus projection in Fig. 28 shows that the addition of very small amounts of BaCl_2 ($\leq 1\%$) does not influence the melting point of the eutectic in a significant way. Further addition of BaCl_2 , however, does quickly lead to an increase of the eutectic temperature.

Acknowledgements

The authors of this paper gratefully acknowledge financial support from the ORANO group, as well as fruitful discussions with Dr Elisa Capelli.

References

- 1 T. Abram and S. Ion, Generation-IV nuclear power: A review of the state of the science, *Energy Policy*, 2008, **36**, 4323–4330.
- 2 D. C. Alders and J. Vlieland, and Thijs, M and Konings, Rudolf Johannes Maria and Smith, Anna Louise. Experimental investigation and thermodynamic assessment of the system, *J. Mol. Liq.*, 2024, 123997.
- 3 O. Beneš, and Konings, Rudolf Johannes Maria. Thermodynamic evaluation of the $\text{NaCl-MgCl}_2\text{-UCl}_3\text{-PuCl}_3$ system, *J. Nucl. Mater.*, 2008, **375**(2), 202–208.
- 4 O. Beneš, R. J. M. Konings, S. Wurzer, M. Sierig and A. Dockendorf, A DSC study of the $\text{NaNO}_3\text{-KNO}_3$ system using an innovative encapsulation technique, *Thermochim. Acta*, 2010, **509**(1–2), 62–66.
- 5 O. Beneš, *Thermodynamic database on molten salt reactor systems. Technical report*, European Commission, Joint Research Centre, 2021.
- 6 E. S. Bettis, R. W. Schroeder, G. A. Cristy, H. W. Savage, R. G. Affel and L. F. Hemphill, The aircraft reactor experimentâ€”design and construction, *Nucl. Sci. Eng.*, 1957, **2**(6), 804–825.
- 7 C. W. Bjorklund, J. G. Reavis, J. A. Leary and K. A. Walsh, Phase equilibria in the binary systems $\text{PuCl}_3\text{-NaCl}$ and $\text{PuCl}_3\text{-LiCl}$, *J. Phys. Chem.*, 1959, **63**(10), 1774–1777.
- 8 G. A. Bukhalova, *Izv. Sek. Fiz.-Khim. Anal.*, 1955, **26**, 138.
- 9 Centre for Research in Computational Thermochemistry. FactSage 7.2.
- 10 P. Chartrand and A. D. Pelton, Thermodynamic evaluation and optimization of the $\text{LiCl-NaCl-KCl-RbCl-CsCl-MgCl}_2\text{-CaCl}_2\text{-SrCl}_2\text{-BaCl}_2$ system using the modified quasichemical model, *Can. Metall. Q.*, 2001, **40**(1), 13–32.
- 11 M. W. Chase Jr, NIST-JANAF thermochemical tables, *J. Phys. Chem. Ref. Data, Monogr.*, 1998, **9**, 737–957.
- 12 H. T. Davis and S. A. Rice, Perturbation theory of the heats of mixing of fused salts, *J. Chem. Phys.*, 1964, **41**(1), 14–24.
- 13 G. Della Gatta, M. J. Richardson, S. M. Sarge and S. Stølen, Standards, calibration, and guidelines in microcalorimetry. Part 2. Calibration standards for differential scanning calorimetry*(IUPAC Technical Report), *Pure Appl. Chem.*, 2006, **78**(7), 1455–1476.
- 14 T. Dumaire, J. A. Ocádiz-Flores, R. J. M. Konings and A. L. Smith, A promising fuel for fast neutron spectrum Molten Salt Reactor: $\text{NaCl-ThCl}_4\text{-PuCl}_3$, *Calphad*, 2022, **79**, 102496.
- 15 A. S. Dworkin and M. A. Bredig, The heats of fusion and transition of alkaline earth and rare earth metal halides, *J. Phys. Chem.*, 1963, **67**(3), 697–698.
- 16 M. Gaune-Escard, A. Bogacz, L. Rycerz and W. Szczepaniak, Calorimetric investigation of $\text{NdCl}_3\text{-MCl}$ liquid mixtures (where M is Na, K, Rb, Cs), *Thermochim. Acta*, 1994, **236**, 67–80.
- 17 H. Gemsky, *Neues Jahrb. Mineral. Geol. Paleontol. Beil.*, 1913, **36**, 513.
- 18 V. P. Glushko and L. V. Gurvich and V. A. Weitz, *et al.*, *Thermodynamic properties of individual substances*, Nauka Publishing House, Moscow, vol. 3, 1978.
- 19 S. A. Hodorowicz, M. Olejak-Chodan and H. A. Eick, A preparatory and X-ray diffraction study of the $\text{SrCl}_2\text{-NdCl}_3$ system, *J. Solid State Chem.*, 1987, **71**(1), 205–213.
- 20 G. W. H. Höhne and H. K. Cammenga, and Eysel, W and Gmelin, E and Hemminger, W. The temperature calibration of scanning calorimeters, *Thermochim. Acta*, 1990, **160**(1), 1–12.
- 21 D. E. Holcomb and G. F. Flanagan and B. W. Patton and J. C. Gehin and R. L. Howard and T. J. Harrison Fast spectrum molten salt reactor options. ORNL/TM-2011/105, 2011.
- 22 K. Igarashi, M. Kosaka, Y. Iwade, T. Hattori and J. Mochinaga, Phase Diagrams of LiCl-NdCl_3 , NaCl-NdCl_3 , and $\text{CaCl}_2\text{-NdCl}_3$ Systems, *Denki Kagaku oyobi Kogyo Butsuri Kagaku*, 1990, **58**(5), 469–470.
- 23 K. W. R. Johnson, M. Kahn and J. A. Leary, Phase equilibria in fused salt systems: binary systems of plutonium (III) chloride with the chlorides of magnesium, calcium, strontium and barium1, *J. Phys. Chem.*, 1961, **65**(12), 2226–2229.
- 24 R. J. M. Konings and A. Kovács, Thermodynamic properties of the lanthanide (III) halides, *Handb. Phys. Chem. Rare Earths*, 2003, **33**, 147–247.
- 25 A. Le Bail, New developments in microstructure analysis via Rietveld refinement, *Adv. X-Ray Anal.*, 2000, **42**, 191–203.
- 26 C. Le Brun, Molten salts and nuclear energy production, *J. Nucl. Mater.*, 2007, **360**(1), 1–5.
- 27 H. L. Lukas and S. G. Fries and B. Sundman, *et al.*, *Computational Thermodynamics: the Calphad method*, Cambridge University Press, vol. 131, 2007.
- 28 J. W. McMurray and K. Johnson and C. Agca and B. R. Betzler and D. J. Kropaczek and T. M. Besmann and D. Andersson and N. Ezell, *Roadmap for thermal property measurements of Molten Salt Reactor systems. Technical*



- report, No. ORNL/SPR-2020/1865, Oak Ridge National Lab.(ORNL), Oak Ridge, TN (United States), 2021.
- 29 G. Meyer and S. Masselmann, The alkali-poor part of the pseudoternary triangle AX/BX₂/MX₃: crystal structures, properties, and potentials of (alkali)/alkaline-earth/rare-earth chloride materials, *Chem. Mater.*, 1998, **10**(10), 2994–3004.
 - 30 I. S. Morozov and F. N. T'en, Types of Equilibrium Diagram of Binary Systems of R.E.E. and Alkaline-earth Metal Chlorides, *Russ. J. Inorg. Chem.*, 1971, **16**(8), 1215–1217.
 - 31 T. Østvold, *A thermodynamic study of some fused salt mixtures containing alkali and alkaline earth chlorides, bromides and iodides, volume 91*, Institute of Physical Chemistry, University of Trondheim, NTH, 1971.
 - 32 G. I. L. van Oudenaren, J. A. Ocadiz-Flores and A. L. Smith, Coupled structural-thermodynamic modelling of the molten salt system NaCl-UCl₃, *J. Mol. Liq.*, 2021, **342**, 117470.
 - 33 A. D. Pelton, P. Chartrand and G. Eriksson, The modified quasi-chemical model: Part IV. Two-sublattice quadruplet approximation, *Metall. Mater. Trans., A*, 2001, **32**(6), 1409–1416.
 - 34 J. Rodriguez-Carvajal, Recent advances in magnetic structure determination by neutron powder diffraction, *Phys. B: Condens. Matter*, 1993, **192**(1–2), 55–69.
 - 35 K. Scholich, *Neues Jahrb. Mineral. Geol.*, 1920, **43**, 269.
 - 36 R. D. Shannon, Revised effective ionic radii and systematic studies of interatomic distances in halides and chalcogenides, *Acta Crystallogr., Sect. A: Cryst. Phys., Diffraction, Theor. Gen. Crystallogr.*, 1976, **32**(5), 751–767.
 - 37 R. A. Sharma and R. A. Rogers, Phase Equilibria and Structural Species in NdCl₃-NaCl, NdCl₃-CaCl₂, PrCl₃-NaCl, and PrCl₃-CaCl₂ Systems, *J. Am. Ceram. Soc.*, 1992, **75**(9), 2484–2490.
 - 38 M. Taube, *Fast reactors using molten chloride salts as fuel. Technical report*, INFCE (Switzerland), 1978.
 - 39 G. Vogel and A. Schneider, Chemie der seltenen erden in geschmolzenen alkalihalogeniden XII [1], *Inorg. Nucl. Chem. Lett.*, 1972, **8**(6), 513–521.
 - 40 E. Vortisch, *Neues Jahrb. Mineral. Geol.*, 1914, **38**, 202–220.
 - 41 J. A. Yingling, J. Schorne-Pinto, M. Aziziha, J. C. Ard, A. M. Mofrad, M. S. Christian, C. M. Dixon and T. M. Besmann, Thermodynamic measurements and assessments for LiCl-NaCl-KCl-UCl₃ systems, *J. Chem. Thermodyn.*, 2023, **179**, 106974.
 - 42 M. A. Zakharchenko and S. M. Aslanov, The ternary system containing the chlorides of lithium, sodium and barium, *Zh. Neorgan. Khim.*, 1963, **8**, 1532–1534.

